CHALMERS
UNIVERSITY OF TECHNOLOGY

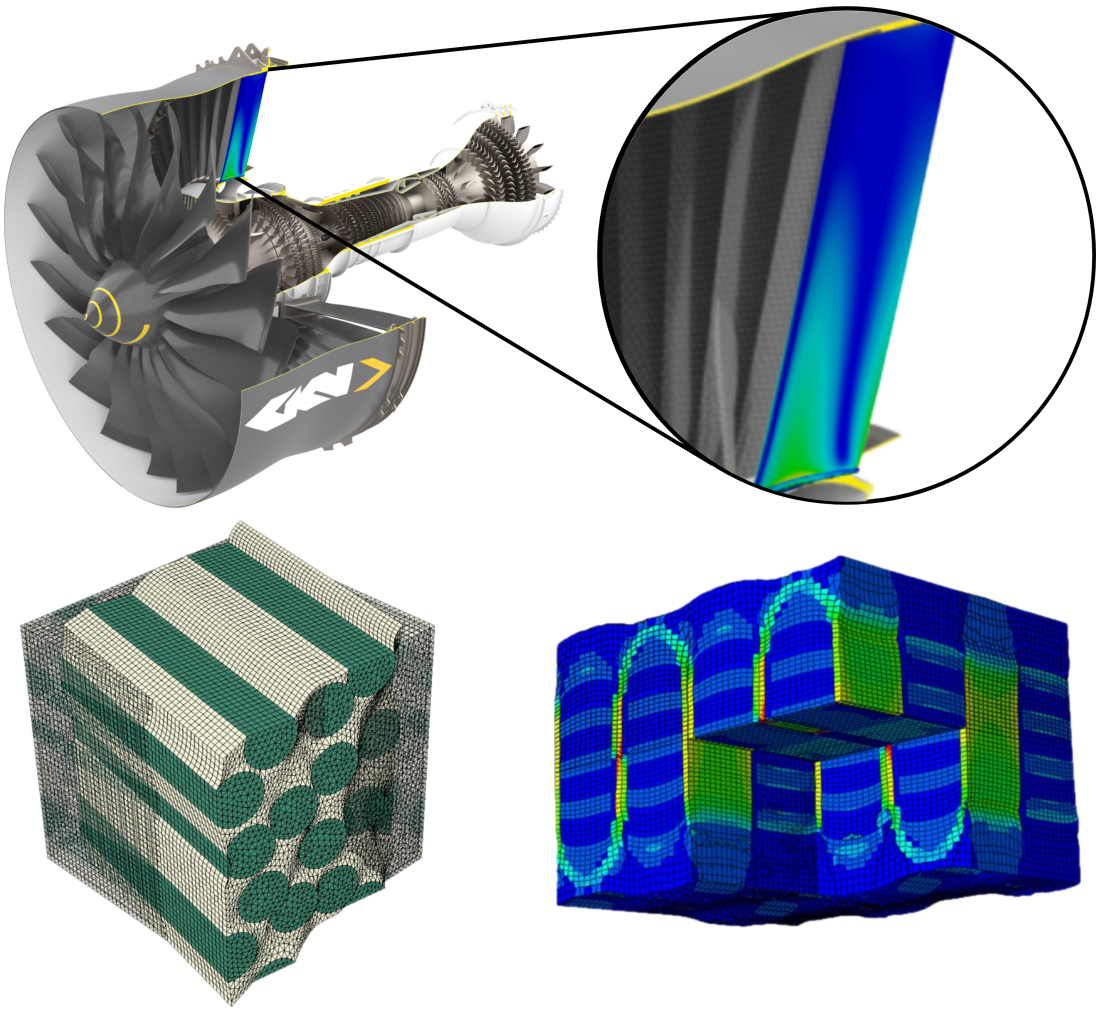

Structural Design and Analysis of a 3D Fabric-Reinforced Composite Outlet Guide Vane

Bachelor's thesis in Mechanical Engineering

Fiona Coates, Walther P. Ericsson, Emily Hughes, Daniel Jinneryd, Jakob Olsson, Anthon Rindsäter

DEPARTMENT OF INDUSTRIAL AND MATERIALS SCIENCE
CHALMERS UNIVERSITY OF TECHNOLOGY
Gothenburg, Sweden 2024
www.chalmers.se

Bachelor's thesis 2024

Structural Design and Analysis of a 3D Fabric-Reinforced Composite Outlet Guide Vane

Fiona Coates, Walther P. Ericsson, Emily Hughes,
Daniel Jinneryd, Jakob Olsson, Anthon Rindsäter

CHALMERS
UNIVERSITY OF TECHNOLOGY

Department of Industrial and Materials Science
Chalmers University of Technology
Gothenburg, Sweden 2024

Structural Design and Analysis of a 3D Fabric-Reinforced Composite Outlet Guide Vane
FIONA COATES, WALTHER P. ERICSSON, EMILY HUGHES,
DANIEL JINNERYD, JAKOB OLSSON, ANTHON RINDSÄTER

Supervisor: Carolyn Oddy, GKN Aerospace AB
Examiner: Magnus Ekh, Department of Industrial and Materials Science

Bachelors's Thesis 2024
Department of Industrial and Materials Science
Chalmers University of Technology
SE-412 96 Gothenburg
Telephone +46 31 772 1000

Cover: A microscale RVE, macroscale RVE and failure criteria on a GKN OGV.

Typeset in LaTeX
Gothenburg, Sweden 2024

Abstract

History shows that commercial airline engines have become larger and heavier. Due to the close relation between engine weight and fuel efficiency, a weight reduction would reduce aviation's carbon footprint. The introduction of composite materials, in particular those with carbon fibre reinforcements, to replace traditional metallic alloys is one avenue to create lighter aeroengines.
This work focuses on an innovative class of composite material with 3D fabric-reinforcement. By having fabric-reinforcement in three dimensions one can overcome a number of challenges found in traditional laminated composite, such as their susceptibility for delamination and poor out-of-plane properties.
The aim of this study is to clarify the mechanical and thermal properties of 3D fabric-reinforced composite materials across different scales. This is in order to propose a final suitable 3D orthogonal non-woven yarn architecture for an Outlet Guide Vane (OGV) in an aero engine. Firstly, the microscale characteristics of these materials are examined, considering the combination of an epoxy matrix and carbon fibres, to provide insights into their mechanical and thermal behaviour. Subsequently, this thesis delves into the mesoscale, integrating micro-mechanical properties of the yarns and polymer matrix properties to tailor the fibre distribution within the yarn structure, aiming to meet the failure criteria on the macroscale. Moreover, it investigates the hypothesis that off-axis yarns enhance shear stiffness moduli, utilising modelling and simulation techniques. Through simulations on the macroscale, the study validates the mechanical elastic properties of the composite material, ensuring its adequacy for the prescribed failure criteria. Furthermore, it predicts and analyses heat transfer effects across the orthogonal non-woven yarn structure when embedded with a thermal element, leveraging calculated thermal properties. Lastly, informed by findings on the macroscale, a final composite yarn structure is proposed that is suitable for application in the designated OGV context. This comprehensive investigation contributes to advancing the understanding of composite materials, particularly in aerospace applications.

Keywords: 3D orthogonal non-woven composite, Failure, Finite element method, Homogenisation, Mechanical properties, Orthotropic, RVE, Textile Structure Modelling, Thermal properties.

Acknowledgements

We would like to thank Carolyn Oddy for providing us with the opportunity and for placing her trust in us with this thesis. She has supported us all the way and we are absolutely in awe of the dedication and insight Carolyn Oddy has shown us. She serves as a role model for each and everyone of us to aspire to be. Further, our gratitude goes out to GKN Aerospace for giving us this opportunity and for their hospitality. They have generously granted us access to their composite laboratory, computing resources, and ANSYS licenses, for which we are grateful. We would like to thank our examiner Magnus Ekh for making this project possible, with his insightful feedback and meticulous attention to detail he has played an important role in shaping the quality of this thesis. To Fureho and Vinnova, thank you for placing your trust in us and making this funded cooperation a reality.

Fiona Coates, Walther P. Ericsson, Emily Hughes, Daniel Jinneryd, Jakob Olsson, Anthon Rindsäter.
Gothenburg, May 2024

Glossary

Below is a glossary that explains the most common terms used in this thesis. It is noteworthy that all definitions have been adjusted to enhance reader comprehension.

1. **3D orthogonal non-woven composites (NOOBED)**: Composite materials that are constructed in three dimensions, where the reinforcing fibres are arranged in an orthogonal (perpendicular) manner and not interlaced between the layers.
2. **ABAQUS**: A finite element analysis software used for engineering simulations.
3. **Aero Engine**: A type of air-breathing jet engine that is widely used in aircraft propulsion.
4. **ANSYS**: Another finite element analysis software used for engineering simulations.
5. **ANSYS Material Designer**: An application in ANSYS, assisting in defining complex material properties.
6. **ANSYS Mechanical**: An application in ANSYS which facilitates FE analysis for examining mechanical systems, structures, and components.
7. **ANSYS Transient Thermal**: An application in ANSYS which determines temperatures and other thermal quantities over time.
8. **Boundary Conditions (BC's)**: Conditions applied to the boundaries of a finite element model to simulate the environment or constraints.
9. **Carbon Fibre-Reinforced Polymers (CFRP)**: Materials made by combining carbon fibre reinforcements with polymer matrix materials.
10. **Convergence Study**: Analysis performed to ensure that the numerical solution obtained from a simulation is stable and accurate.
11. **Failure Criteria(FC)**: Predicts material failure under multiaxial stress.
12. **Finite Element (FE) Analysis**: A computational method used to approximate and analyse the behavior of structures under various conditions.
13. **Isotropic**: A material with uniform properties in all directions.
14. **Linear Elasticity**: The behavior of materials that return to their original shape after deformation when subjected to loads.
15. **Macroscale**: The largest scale in a hierarchical modeling approach, dealing with the overall system or structure.
16. **Mesoscale**: An intermediate scale between microscale and macroscale, considering larger assemblies or structures.

17. **Microscale**: The smallest scale in a hierarchical modeling approach, focusing on individual components or elements.
18. **Orthotropic**: Materials with varying mechanical properties in different directions.
19. **Outlet Guide Vanes (OGV)**: Components in a turbine engine that provides structural support and guides airflow to improve engine efficiency.
20. **Representative Volume Element (RVE)**: A small sample that represents the microstructure of a material.
21. **Resin**: A binding agent used in composite materials to hold reinforcing fibres together. Resins undergo curing processes to provide structural integrity to the composite.
22. **Stiffness Matrix**: A mathematical representation of the relationship between applied forces and resulting displacements in a structure.
23. **TexGen**: An open-source software for modelling textile structures.
24. **Transversely Isotropic**: Material with consistent properties along one axis but varying properties perpendicular to it.

Contents

List of Figures

List of Tables

1
Introduction

1.1 Background

Today's commercial airline engines are becoming larger as a consequence of the optimisation of the aero engine [1]. A trade-off between the more fuel efficient fan thrust and the more powerful jet thrust leads to larger fan blades and therefore increased sizes of the engine diameter. Due to the overlapping relations between engine weight and fuel efficiency, reducing the weight of the individual parts would entail further optimisation of the performance of an aero engine. One component in an aircraft engine that affects the weight are the outlet guide vanes (OGVs) seen in Figure 1.1, which are primarily made from metallic alloys. The OGVs serve two purposes: they form a structural connection between the main engine housing and the aircraft attachment point as well as steer the flow coming from the low-pressure turbine into the axial outflow [2]. The developed OGV in this thesis is only a model strictly created for research and development purposes.

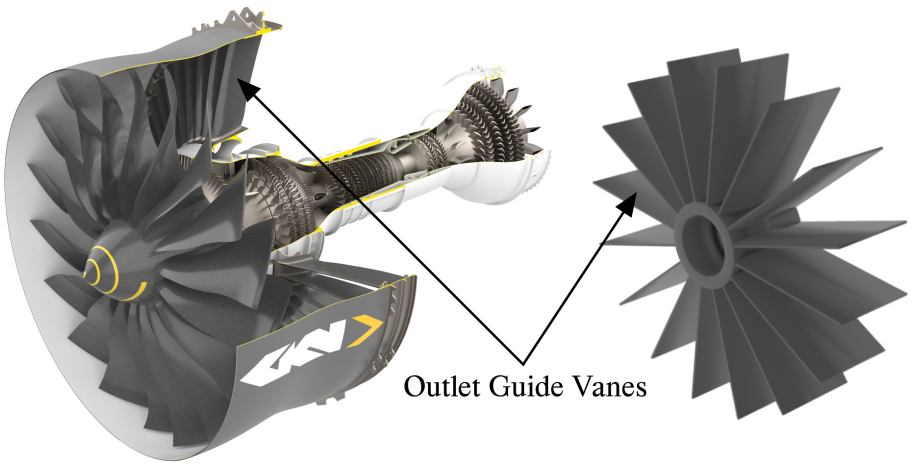

Figure 1.1: *Illustration of an aero engine (left) and outlet guide vanes (right). [3]. Adapted with permission.*

The use of carbon fibre-reinforced polymers (CFRPs) instead of metallic alloys can reduce the overall weight of the engine, leading to an increase in fuel efficiency. This bachelor thesis was conducted in collaboration with GKN Aerospace AB, a leading global aerospace supplier for aircraft manufacturers [4]. Additionally, it involved collaboration with Fureho AB, specialising in the design, development, and manufacturing of near-net shape 3D composite preforms [5].

Many promising mechanical properties are exhibited by CFRPs. This includes high stiffness and strength relative to weight and excellent fatigue resistance compared to many common metallic alloys [6]. Laminated composites are the most traditional fibre-reinforced composite material found on the market. This generally involves layering unidirectional (UD) materials to achieve high in-plane performance. However, by having carbon fibres aligned in three orthogonal independent directions and embedded in resin, one can further increase the through-thickness mechanical properties. These materials, known as 3D fabric-reinforced polymers, enable high specific in-plane and out-of-plane stiffness and strength properties, as well as high fracture toughness and damage tolerance, when compared to UD composites.

Due to the structure of the 3D CFRPs, it is possible to tailor the distribution of the fibre reinforcements in specific directions. This gives them a favourable response to impact and complex loading scenarios. Furthermore, the fabric preforms can be produced in near-net shapes. Compared to traditional laminated composites, this approach drastically reduces labour and joining needs, enabling a substantial reduction in material waste [7]. These materials have primarily been developed by the aerospace industry to meet high structural demands, reduce emissions and fabrication costs.

Composites with 3D fabric-reinforcements can be divided into six subgroups: braided, knitted, stitched, z-pinned, non-woven, and woven [6]. This study will focus on 3D orthogonal non-woven composites using carbon fibres, also known as Noobed 3D Fabric pre-forms (see Figure 1.2), and the development of the necessary analysis tools needed to be able to predict the material's mechanical performance.

Figure 1.2: *Noobed 3D Fabric pre-form. [5]. Reprinted with permission.*

1.2 Material Modelling

Presented in this section is an analysis of 3D fabric-reinforced composites across micro-, meso-, and macroscales. It defines isotropic, transversely isotropic and orthotropic materials, whilst also discussing the use of representative volume elements (RVEs). Finally, the implementation of periodic boundary conditions (PBCs) is outlined.

1.2.1 Description of Micro-, Meso- and Macroscale

Composites with 3D fabric-reinforcements are hierarchical in nature. In order to analyse their mechanical properties it is necessary to consider their behaviour at multiple scales. The three sub-scale considered in this analysis are the micro-, meso- and macroscale, illustrated in Figure 1.3. The coordinate systems used in Figure 1.3 are specific for each of the three scales and will be consistently referred to throughout the report: the microscale uses the coordinate system $[x, y, z]$, the mesoscale uses the coordinate system $[1, 2, 3]$ and the macroscale uses the coordinate system $[i, j, k]$.

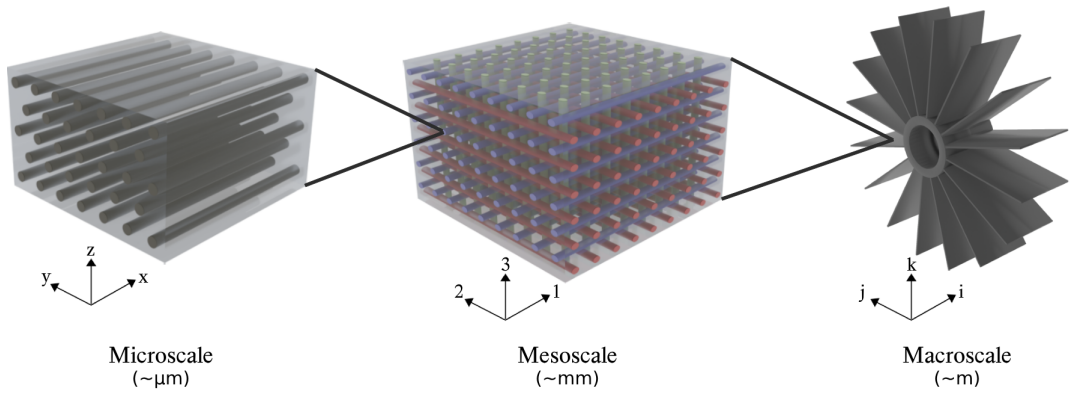

Figure 1.3: *Illustrative models presented from left to right, representing the micro-, meso-, and macroscale and their approximate dimensions.*

The microscale FE model investigates the material behaviour at the scale of individual carbon fibres surrounded by the polymer matrix. This is representative of an impregnated carbon fibre yarn. At the mesocale, the architecture of the 3D yarn structure is considered and is again modelled considering a polymer matrix surrounding the yarns. On the macroscale, a full component is considered and is assumed to have homogeneous properties.

1.2.2 Definitions of Isotropic, Transversely Isotropic and Orthotropic Materials

In order to describe the material behaviour on different scales it is necessary to understand how to classify material properties. In this work, references are made to isotropic, transversely isotropic and orthotropic materials. The three considered material characteristics are illustrated in Figure 1.4.

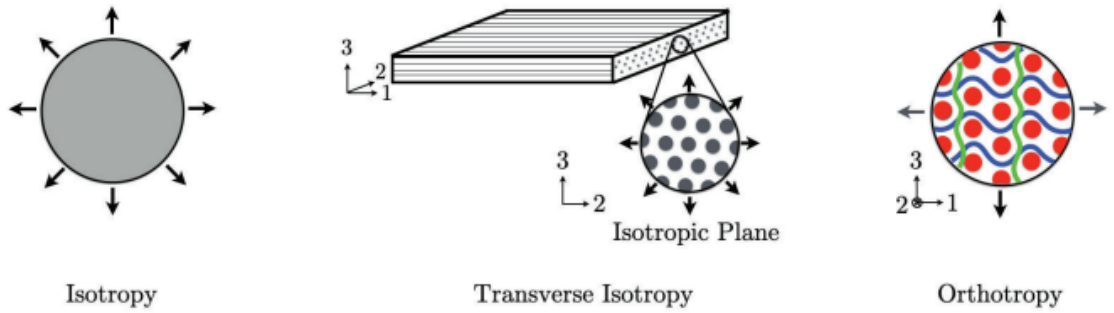

Figure 1.4: *An illustration of isotropy, transverse isotropy and orthotropy. [7]. Reprinted with permission.*

The 3D composite on the macroscale can be described as an orthotropic material [7]. Orthotropic materials have three preferred directions, each with unique material properties. The orthotropic stiffness matrix describes the elastic relationship between the elastic properties for each direction in the local arbitrary coordinate system [*1, 2, 3*] which can be seen in both Figure 1.3 and 1.4. This implies that each direction has its own material properties. Note that the differentiation here is not made between the coordinate systems indicated in each scale in Section 1.2.1. Most generically, this section will only consider a material in an arbitrary [*1, 2, 3*] coordinate system. Firstly, orthotropic materials need nine elastic properties. These nine properties are Young's moduli for the directions E_1, E_2, E_3, stiffness moduli in shear G_{12}, G_{23}, G_{31}, and Poisson's ratios ν_{12}, ν_{23} and ν_{31}. The orthotropic stiffness matrix can in Voigt form be expressed as

$$\begin{bmatrix}\sigma_{11}\\ \sigma_{22}\\ \sigma_{33}\\ \sigma_{23}\\ \sigma_{31}\\ \sigma_{12}\end{bmatrix} = \begin{bmatrix} \frac{E_1(1-\nu_{32}\nu_{23})}{\Delta} & \frac{E_1(\nu_{21}+\nu_{31}\nu_{23})}{\Delta} & \frac{E_1(\nu_{31}+\nu_{21}\nu_{32})}{\Delta} & 0 & 0 & 0 \\ \frac{E_2(\nu_{12}+\nu_{13}\nu_{32})}{\Delta} & \frac{E_2(1-\nu_{31}\nu_{13})}{\Delta} & \frac{E_2(\nu_{12}+\nu_{13}\nu_{32})}{\Delta} & 0 & 0 & 0 \\ \frac{E_3(\nu_{13}+\nu_{12}\nu_{32})}{\Delta} & \frac{E_3(\nu_{23}+\nu_{13}\nu_{21})}{\Delta} & \frac{E_3(1-\nu_{12}\nu_{21})}{\Delta} & 0 & 0 & 0 \\ 0 & 0 & 0 & G_{23} & 0 & 0 \\ 0 & 0 & 0 & 0 & G_{31} & 0 \\ 0 & 0 & 0 & 0 & 0 & G_{12} \end{bmatrix} \begin{bmatrix}\varepsilon_{11}\\ \varepsilon_{22}\\ \varepsilon_{33}\\ \gamma_{23}\\ \gamma_{31}\\ \gamma_{12}\end{bmatrix}, \quad (1.1)$$

where Δ is defined as

$$\Delta = 1 - \nu_{12}\nu_{21} - \nu_{23}\nu_{32} - \nu_{31}\nu_{13} - 2\nu_{12}\nu_{23}\nu_{31}. \quad (1.2)$$

The yarns on the mesoscale are generally described using transverse isotropy. This means that it contains one plane of symmetry, as shown in Figure 1.4 [7]. The required stiffness properties are then the Young's modulus in the fibre direction E_1, the Young's modulus transverse to the fibre direction $E_2 = E_3$ and the shear modulus in the non-isotropic planes $G_{12} = G_{13}$. The last two properties are the Poisson's ratios ν_{23} and $\nu_{12} = \nu_{13}$.

On the microscale, individual carbon fibres and the epoxy matrix are generally considered to be isotropic. This means they have the same response in all three directions, as shown in Figure 1.4. Only two material parameters are needed to describe

isotropic mechanical behaviour, E and ν. The materials used for the microscale FE simulations, T700G (carbon fibre) and RTM6 (epoxy matrix), are presented in Table 1.1. The thermal conductivity k, and specific heat c_p, characterise the thermal behaviour of the materials.

Table 1.1: Input material properties.

Material	E [GPa]	ν [-]	ρ [kg/m^3]	k [W/mK]	c_p [J/kgK]
Carbon Fibre *T700G*	240	0.31	1800	9.6	752
Epoxy Resin *RTM6*	3.4	0.3	1140	0.2*	2160

*Standard value for thermal conductivity of epoxy resin at room temperature [8].

Table 1.2 summarises each constituents material properties and the homogenised response of each scale.

Table 1.2: Material properties of each constituent and the homogeneous outcome.

	Microscale	Mesoscale	Macroscale
Fibre/Yarn	Isotropic	Transv. isotropic	Orthotropic composite
Matrix	Isotropic	Isotropic	
Homogenised response	Transv. isotropic	Orthotropic	

1.2.3 Representative Volume Elements for Acquiring Material Properties

As previously outlined, the properties of materials vary depending on the scale at which they are observed. It then becomes imperative to have the ability to predict the material stiffness tensor at different scales in order to feed this information to the scale above it. One method to do this is through the use of a representative volume element (RVE), which is the smallest repeating volume that is representative of the material behaviour and allows for extracting representative material properties [6]. The common approach to estimating mechanical properties of a carbon fibre-reinforced composite, on the micro- and mesoscales, involves using numerical methods such as the Finite Element Method on the smallest RVE [9]. By setting up a finite element (FE) model on the RVE with load cases that isolate and capture each unidirectional stress-strain response, one can extract the anisotropic material parameters. More specifically, Figure 1.5 illustrates the isolated load cases to extract such parameters for an orthotropic material. The engineering constants predicted, are the nine elastic properties needed for the stiffness matrix defined in Eq. (1.1). Presented in the figures are the extracted constants for the respective load cases of the RVE. The influence of the constituents difference in stiffness is visible in the lower load cases, allowing the RVE to deform freely at the surfaces.

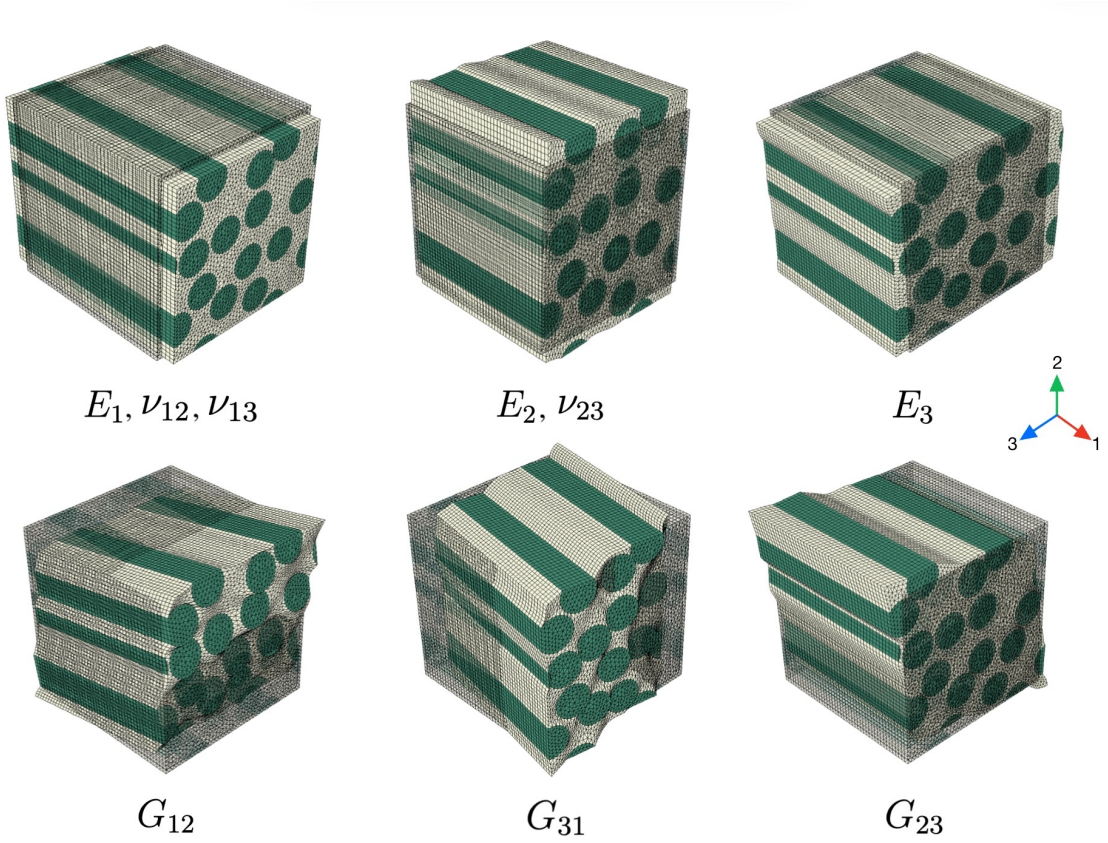

Figure 1.5: *A representation of displacement induced by the periodic boundary conditions on an RVE to estimate effective elastic properties. The green constituent is a carbon fibre strand and the light one is epoxy.*

More specifically, in a mathematical sense, the homogenised RVE properties can be computed using the Iso-strain method. After applying one of the deformation modes shown in Figure 1.5, the macroscopic averaged stress and strain denoted $\bar{\boldsymbol{\sigma}}$ and $\bar{\boldsymbol{\varepsilon}}$ over the RVE domain Ω can be calculated using the individual stress and strain components in each integration point, denoted $\boldsymbol{\sigma}$ and $\boldsymbol{\varepsilon}$. In index form where the subscripts denote each component, i.e. i,j = 1,2,3, this average is calculated as

$$\overline{\sigma}_{ij} = \frac{1}{\Omega}\int_{\Omega} \sigma_{ij} d\Omega, \quad \overline{\varepsilon}_{ij} = \frac{1}{\Omega}\int_{\Omega} \varepsilon_{ij} d\Omega, \tag{1.3}$$

in accordance with [6].

Then, from six independent global strain and stress vectors, it is possible to solve for the homogenised stiffness matrix according to

$$\overline{\boldsymbol{\sigma}} = [\overline{\boldsymbol{C}}]\overline{\boldsymbol{\varepsilon}}. \tag{1.4}$$

The stiffness matrix $[\overline{\boldsymbol{C}}]$ contains elastic stiffness constants which vary based on the scale represented by the RVE and have been discussed in Section 1.2.2.

In the context of material homogenization, boundary conditions (BCs) play a critical role. The standard use of traditional Dirichlet and Neumann boundary conditions prescribed to a surface are inadequate for analysing RVEs and their

homogenised response. For these cases, periodic boundary conditions (PBCs) are preferably utilised to prevent over-constraining the RVE and thereby overestimating its elastic properties [10].

Consequently, for orthotropic materials, Eq. (1.1) can be used as Eq. (1.4) to represent the stress-strain relationship. By subjecting the RVE to periodic displacements on its sides, it becomes feasible to solve for each term in the stiffness matrix since displacements are defined and stresses can be calculated.

To implement periodic constraints in commercial FE software, the concept proposed by [10] and adapted by [11] in the EasyPBC plugin for ABAQUS can be employed. This plugin automates the creation and linking of sets to establish deformable periodic boundary surfaces. However, instead of averaging the stress tensor over the domain, EasyPBC determines the average stress tensor by solving for the reaction forces over the displaced surface. ANSYS provides an application called Material Designer for its users which is a sophisticated RVE modeller built into the program.

A limitation of PBCs in EasyPBC and Material Designer is the requirement of a periodic mesh, which demands identical nodes on opposing sides for consistent displacement. Figure 1.6a illustrates a non-periodic mesh, while Figure 1.6b displays a periodic mesh with identical nodes on the opposing sides.

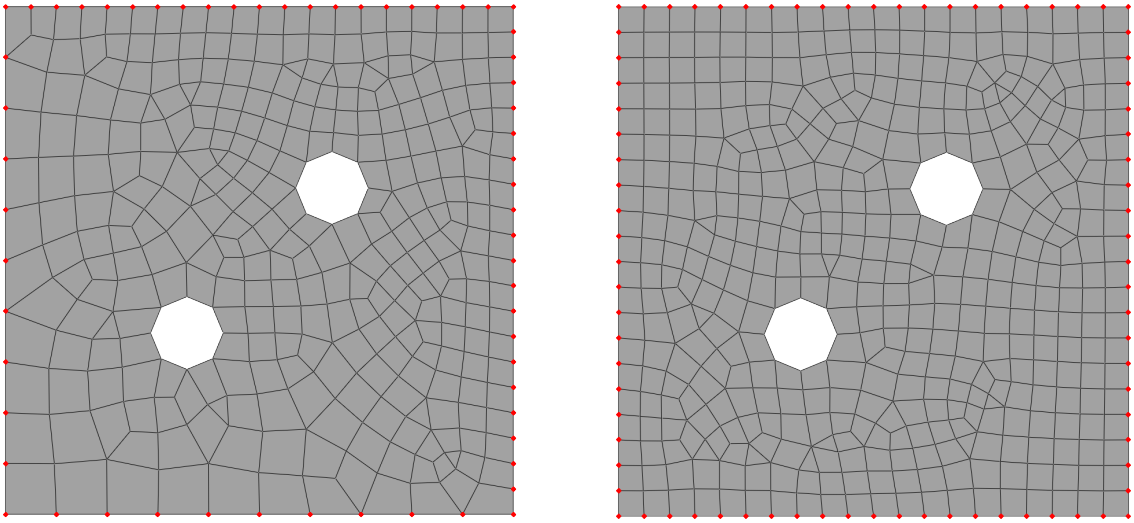

(a) *Non-Periodic Mesh.* **(b)** *Periodic mesh.*

Figure 1.6: *Representation of a non-periodic mesh (a) and a periodic mesh (b). Along the outer surface the nodes are marked to emphasise the difference.*

1.3 Project Scope

The following section outlines the objectives and workflow that guided the project, along with a discussion of the limitations and ethical considerations. Additionally, a brief overview of the use of artificial intelligence in the project is provided.

1.3.1 Goals

In order to further drive the use of 3D-fabric reinforced composites, analysis tools are required in order to predict their mechanical response. With the overall aim of analysing an OGV manufactured using 3D-fabric reinforcements, the goals of this thesis are as follows:

Macroscale:

- Create an FE analysis tool for analysing the mechanical elastic properties for the 3D orthogonal non-woven composite designed on the mesoscale.
- Implement local element orientations to include the impact of local yarn alignments in the OGV.
- Formulate and evaluate a failure criteria (FC) to assess the designed material's mechanical properties.

Mesoscale:

- Develop an analysis tool using FE models of representative volume elements to predict the orthotropic elastic material properties of various yarn architectures of a 3D orthogonal non-woven composite.
- Explore methods to produce a mesh for the 3D orthogonal non-woven composite model that can be used with the ABAQUS plugin EasyPBC, i.e. a periodic mesh.
- Taken into account the micro-mechanical properties for the yarns and the properties for the polymer matrix, tailor and iterate the yarn distribution in a 3D orthogonal non-woven yarn structure that is sufficient to satisfy the failure criteria on the macroscale.
- Model and simulate a textile with off-axis (45°) yarns to explore the hypothesis that off-axis yarns in a 3D orthogonal non-woven yarn structure increase the shear stiffness moduli.

Microscale:

- Develop an analysis tool using FE models of representative volume elements that can extract elastic mechanical and thermal properties on the microscale.
- Use the FE models to predict the variation in mechanical properties depending on fibre volume fraction. Provide these results to the mesoscale.
- Use the FE models to predict the variation in thermal conductivity for varying fibre volume fractions on the microscale. Use these results to predict and present the effects of heat transfer across the OGV surface when a thermal element is embedded into the microstructure.

1.3.2 Workflow

The overall information flow is illustrated in Figure 1.7. As the work is divided into three different scales, each dependent on the other, the information is streamlined, beginning with the supplied inputs for the microscale constituent material properties RTM6 and T700G, as presented in 1.2.2. In order to better visualise and understand the workflow in detail, see A.1.

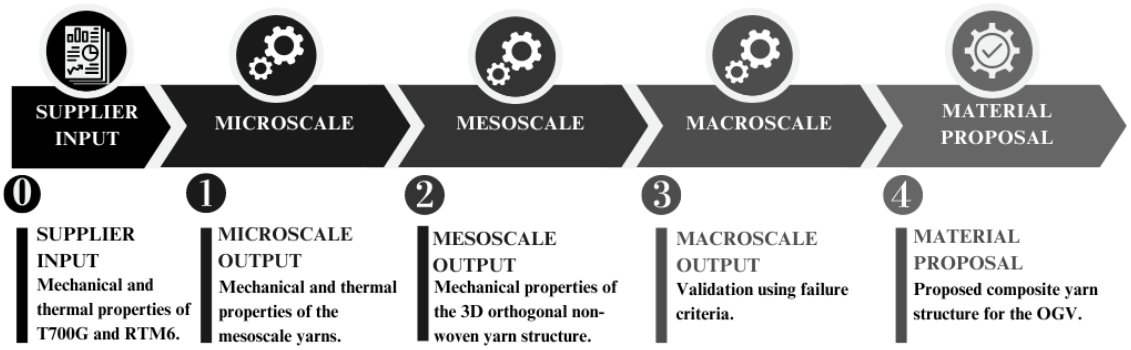

Figure 1.7: *Illustration of the streamlined information flow.*

1.3.3 Limitations

The project will be conducted under the following limitations:

- The FE model will exclusively consider linear-elastic behaviour. Non-linear effects due to damage, plasticity or viscosity will not be considered. When analysing failure criteria, a robust safety margin is consider to account for this simplification.
- The external geometry of the CAD model of the OGV that was provided cannot be modified since it is an aerodynamic surface.
- Only idealised RVE geometries will be considered on the micro- and mesoscale. This is to reduce the computational complexity of the model and simplify the FE analysis.
- Only one resin type, RTM6, and one carbon fibre type, T700G, are considered at the micro-, meso-, and macroscales.
- Additionally, the thesis has a time limit, with a completion deadline set for the end of spring, which spans a total of 19 weeks.

1.3.4 Ethical and Environmental Aspects

The aerospace industry's environmental impact raises ethical questions about the necessity of flight. While lightweight components can reduce emissions, it prompts debate on the overall sustainability of air travel. Advancements in lighter transportation could facilitate a shift to sustainable energy sources like electric or BIO-fuel, fostering innovation and reducing fuel consumption.

This analysis focuses on CFRP, which can provide substantial weight reduction opportunities, saving energy and reducing emission especially over the lifetime of a component. However, they do still pose environmental challenges which is an ongoing research area. These challenges include limited recycling and high CO_2 emissions during production of the carbon fibres. Sustainable production methods for CFRP can mitigate these issues.

The thesis is purely aimed at the application of composite materials to commercial aircraft engines. However, it should be stated that GKN is involved in the development of governmental and defence solutions and that the development of technology related to CFRPs can be classified as dual-use and may be applied to

both civilian and defence applications.

1.3.5 Usage of Artificial Intelligence

Artificial intelligence has been used to enhance the language and achieve a consistent writing style. Specifically, DeepL will be used for its academic writing style assistance [12]. ChatGPT by OpenAI has also been utilised to create a glossary explaining technical terms [13]. The glossary has then been revised by the project group.

2

Macroscale

In order to assess the mechanical performance of the composites, an FE model was constructed in ANSYS Mechanical in order to capture the effects of the material. The model was used to compute the strains, which can be defined by the user in the form of a failure criteria (FC). The macroscale utilises the [*i, j, k*] coordinate system.

2.1 The Macroscale FE Model

The CAD model of the vane was accompanied by two fixtures which constrained the OGV via fixed surface contact. The OGV and fixtures were modelled using second-order tetrahedral elements, as this allowed the use of the Augmented Lagrangian method to apply contact between the OGV and fixtures in the most effective manner. A convergence study was conducted to determine the element sizing. The BC's were applied to the fixtures and an illustration of the meshed OGV part with the corresponding fixtures is shown in Figure 2.1. In the figure, **A** represents the fixed BC. On surface **B**, forces were applied in the *i*, *j* and *k* directions. The normalised values of these were 1, 0.079 and 0.211, respectively. A uniform, undisclosed pressure was applied over the entire OGV surface.

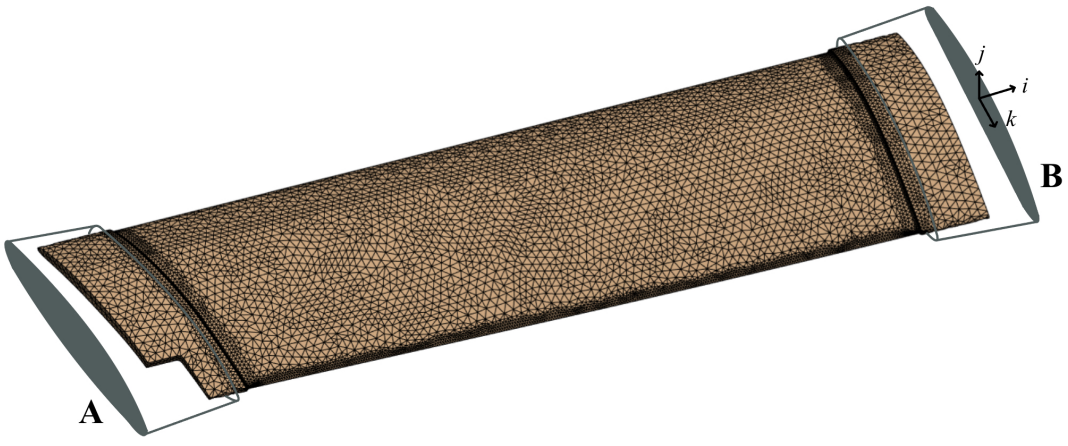

Figure 2.1: *The mesh of the OGV is depicted with illustrated fixtures. The **A** marks the fixed BC at the shaded surface. The **B** marks the normalised forces along the i, j and k directions, applied at the shaded surface.*

Two significant challenges had to be addressed when developing the model. Firstly,

the assumption that global material properties would remain constant throughout the model was not realistic. Therefore, the use of element orientation was implemented to more accurately describe the orthotropic material properties that followed the curved surface of the OGV. Secondly, there is no universal way to define a FC for the composite. A user-defined FC, Eq. (2.1), was created to evaluate the strain in each element's local coordinate system and will be explained in Section 2.2.2. To evaluate the performance of the composite in the OGV, the region under the fixtures and the fixtures themselves were excluded from the FC, which can be visualised in Figure 2.3.

There was close collaboration between the meso- and macroscale. The macroscale provided stiffness guidelines for the mesoscale model and validated material suggestions provided by the mesoscale so that the OGV would not exceed the maximum FC.

2.2 Tools for Macroscale Modelling and Analysis

In order to propose a suitable yarn architecture, an FE model of the OGV was constructed to capture the behaviour of the part under loading with the suggested materials applied. This section presents the methods to validate the materials with the help of failure criteria and the use of element orientation in ANSYS Mechanical.

2.2.1 Element Orientation

To ensure an accurate representation of the material's behaviour, it is essential that the material properties in each element align with the direction that the real material would exhibit. The curved surface, such as that of the OGV, will have a material that behaves differently from the global coordinate system. This phenomenon does not affect isotropic materials, but it will affect orthotropic ones, as their properties depend on the element's orientation, which in turn defines the material properties for that specific element. To illustrate this further, consider the case shown in Figure 2.2 which has the local element coordinate system [*1, 2, 3*]. Note how the *1*-direction (red arrow), *2*-direction (green arrow) and *3*-direction (out of plane) can be defined however the user wants, as seen to the right, while the left follows the global coordinate system. This property is vital in capturing the behaviour of the material in the OGV model. A local coordinate system that closely resembles the right side of Figure 2.2, which is utilising the global coordinate system on the mesoscale as illustrated in Figure 1.3, defined the element orientation.

2.2.2 Failure Criteria

The design of failure criteria for the considered class of composite materials remains an ongoing research area. However, final failure of a component usually takes place when the reinforcement yarns snap. This is usually dictated by the maximum allowable strain being overcome. Therefore, a strain-based failure criteria was used in order to evaluate against known material parameters. The failure criteria considered here account for the orthotropic nature of the 3D-fabric reinforcements. The user

must supply the maximum allowable strain for each reinforcement direction and in each shear plane. These are denoted as ε'_1, ε'_2, ε'_3, ε'_{12}, ε'_{13} and ε'_{23}. The failure criteria can then be stated as

$$FC = \sqrt{\left(\frac{\varepsilon_1}{\varepsilon'_1}\right)^2 + \left(\frac{\varepsilon_2}{\varepsilon'_2}\right)^2 + \left(\frac{\varepsilon_3}{\varepsilon'_3}\right)^2 + \left(\frac{\varepsilon_{12}}{\varepsilon'_{12}}\right)^2 + \left(\frac{\varepsilon_{13}}{\varepsilon'_{13}}\right)^2 + \left(\frac{\varepsilon_{23}}{\varepsilon'_{23}}\right)^2}. \tag{2.1}$$

This implies that when the failure criteria reaches a value of 1 in an element, the component is assumed to have failed in that element.

The FC was evaluated with the option averaged, for integration points results. The CAD model of the vane exhibited minor geometric discontinuities in regions of interest. Therefore, the averaging process served to smooth the values in these regions.

Following internal discussions with GKN Aerospace, it was determined that the axial strain limit ε'_1, ε'_2 and ε'_3 could be considered to be 1% and the shear strain limit ε'_{12}, ε'_{13} and ε'_{23} to be 5% as a guideline [3]. The estimate provided is a highly conservative result intended to facilitate arbitrary comparisons of material properties. An illustrative example of failure criteria over the OGV can be observed in Figure 2.3.

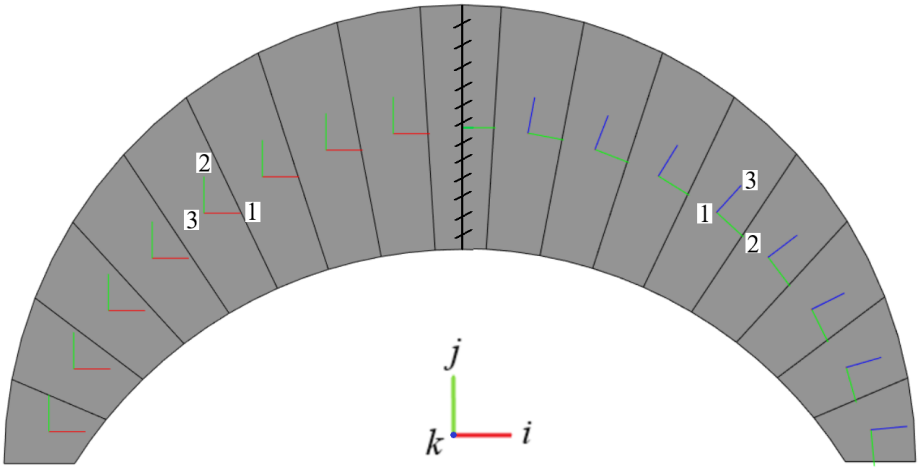

Figure 2.2: *Comparison between global and user defined element orientation in an arbitrary geometry. The global coordinate system is defined [i, j, k] and the local element coordinate system is defined by [1, 2, 3]. Left side: element orientation defined by the global coordinate system. Right side: element orientation defined by the curvature of the surface.*

2.3 Macroscale Results and Discussion

A solution will be presented for one type of the composite material in question, accompanied by an analysis of potential sources of error and areas for improvement.

2.3.1 Failure Criteria on the Macroscale Model

An example of the FC with a material that contains a distribution of 55-33-12% of the reinforcement yarns in the *1, 2* and *3* directions will be presented. This material will be introduced in Section 3.3.2. The model exhibited a low strain globally, but experienced a high strain locally, leading to a global maximum FC in a critical region. The FC over the OGV and the critical region is visualised in Figure 2.3. The critical region was of a very small size, which is a cause for concern with respect to fatigue. This is due to the risk for crack initiation, crack propagation and ultimately fracture. The mesh of the critical region is shown in the bottom right in order to visualise the refinement needed to capture the local FC.

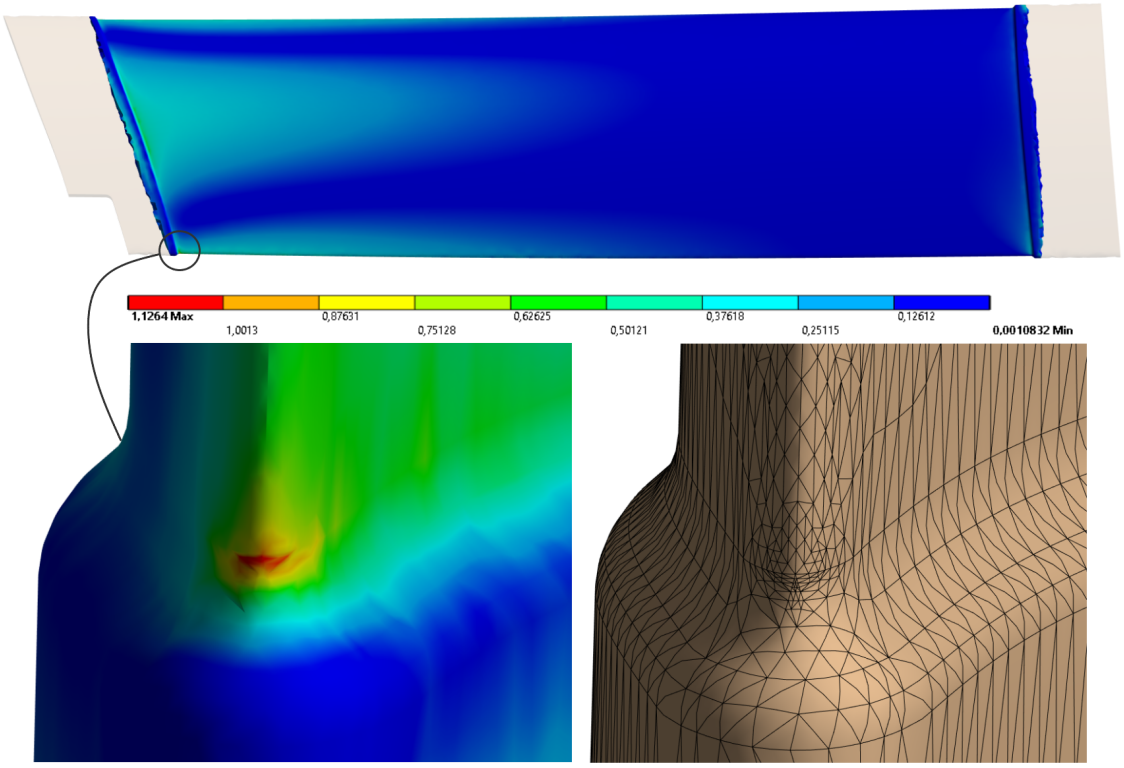

Figure 2.3: *The figure visualises the FC [-] evaluated using averaged integration points on the OGV. The close up pictures of the OGV on the bottom, shows the FC in the critical region along with the mesh of the region.*

2.3.2 Macroscale Model Uncertainties and Sources of Error

Evaluating the maximum FC in the model may result in inaccurate outcomes if the affected elements are below standard in terms of quality or if they fail to capture the varying gradients within the model. This could lead to the FC being either over- or underestimated in the affected elements. It is possible to define an average FC over the critical region (the expanded region in Figure 2.3). However, the decision was ultimately made to evaluate the maximum FC over the averaged integration points because there was a very high spike in the FC locally, but the surrounding material

was well below the upper limit. Consequently, the decision to include this spike in the critical region was based on the assumption that if a crack were to initiate in the material, this would be the location where the risk would be greatest.

The best found approach for modelling the fixtures involved the use of tetrahedral elements to circumvent contact issues between OGV and fixtures. However, it is possible that other elements could yield more accurate results. A comparison between tetrahedral and hexahedral elements could prove beneficial. This could be achieved through the use of static condensation, which entails representing the fixtures of the entire model as their stiffness equivalent, thus allowing for more detailed modelling of each part. Thereby, opening up another avenue for circumventing the contact issues.

The material near the surfaces and especially around heavily curved ones, are in fact, not entirely composed of the same material as the entire OGV. In reality, the material is not homogeneous, nor linear elastic and would be affected by softening from resin pockets. Consequently, the region exhibiting the highest FC would have different properties, thereby, a different response. The CAD model does not have a purely smooth transition and instead has sharp edges in the vicinity of the critical region where this sheet of softer composite would begin to layer. The sharp edge transition can be observed in Figure 2.4. If a softer material were to be assigned to this region, the force path would change in the critical region, resulting in a change in the FC. Given the absence of experimental data to correlate the mathematical model to reality for this class of composites, the FC remains unweighted. A more accurate FC could be achieved by using experimental values to accurately weigh the terms.

In general, the FC is below the assigned limit. Given that the material is freely designed, local reinforcements could be implemented to reduce the peak strain, thereby lowering the maximum FC.

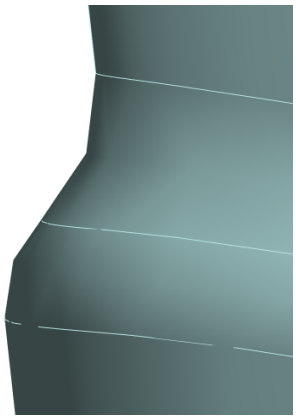

Figure 2.4: *A visualisation of how the geometry does not have completely smooth geometric transitions in the critical region.*

3

Mesoscale

The mesoscale acts as a bridge between the microscale and macroscale, as its structure directly impacts the properties of the OGV and it uses the elastic properties from the microscale analysis. This chapter focuses on the theoretical framework necessary to develop the proposed yarn architecture in the material, as well as the method utilised to tailor the fibre distribution in the composite given the load case on the OGV.

3.1 3D Orthogonal Non-Woven Fabrics

In a 3D orthogonal non-woven fabric, the yarns are oriented in the three orthogonal directions within the [*1, 2, 3*] coordinate system. Figure 3.1 illustrates the yarn structure for an arbitrary textile as well as the RVE from that textile. As previously stated, the RVE is the smallest repeating volume element that represents the properties for the whole textile. By placing copies of the RVE in Figure 3.1b beside each other in directions *1*, *2*, and *3*, the textile model in Figure 3.1a can be constructed, with the exception of the top and bottom curves in the through thickness yarns, which run over the yarns in direction *1*. This will be further discussed in Section 3.3.3.

Throughout the report the red yarns will be referred to as the *yarns in direction 1*, the green yarns will be referred to as *yarns in direction 2* and the blue yarns will be referred to either as *through thickness yarns* or *through thickness reinforcement*.

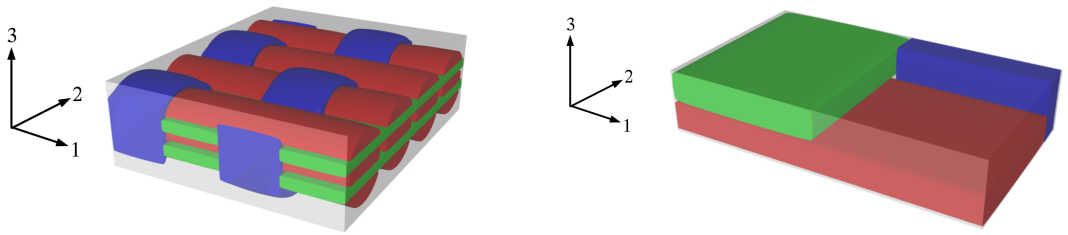

(a) *Yarn structure of a textile model.* **(b)** *Yarn structure of an RVE.*

Figure 3.1: *Yarn structure.*

For all modelled yarns, each yarn is comprised of 12,000 individual fibres with a diameter of 7 μm [3]. The elastic properties of the yarns are derived from the microscale analysis, as elaborated upon in Section 4.1. The foundation for the mesoscale RVEs were given by Fureho [14].

In reality, yarns take on various shapes as they are compacted between one another [6]. As illustrated in Figure 3.2, these can range from more cylindrical cross sections to more rectangular cross sections and everything in between. However, in this analysis idealised yarn geometries will be considered.

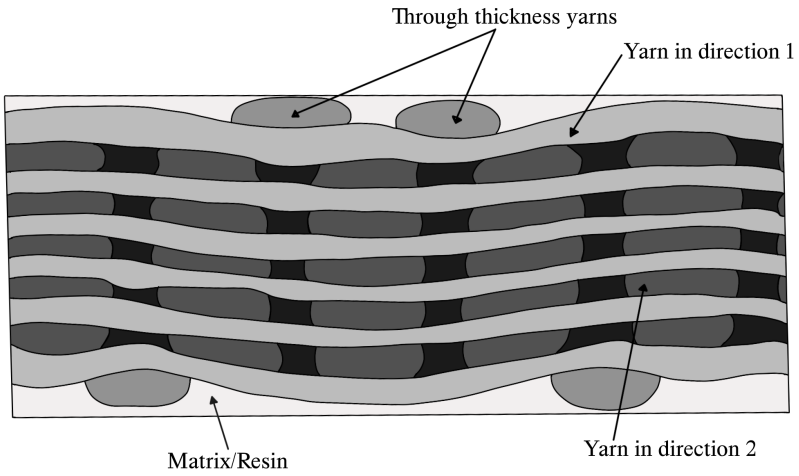

Figure 3.2: *Sketch of a micrograph of the realistic yarn structure in a 3D orthogonal non-woven CFRP. Illustration based on [6].*

In the context of textile models, the term "yarn fibre volume fraction" (V_f) refers to the proportion of carbon fibres in the yarn relative to the amount of polymer matrix. Similarly, the term "domain fibre volume fraction" ($V_{f,d}$) refers to the proportion of carbon fibres in the RVE or textile relative to the amount of polymer matrix. The term "fibre distribution" (FD) is used to describe the proportion of fibres in the RVE or textile that are oriented in specific direction, for example 60% in direction *1* (FD_1), 30% in direction *2* (FD_2) and 10% in direction *3* (FD_3). The yarn fibre volume fraction typically has an approximate value of 60% in each yarn, while the domain fibre volume fraction has a value of 40-50%. The fibre distribution can be tailored in a multitude of ways to suit specific load cases.

The most commonly used upper limit for these parameters is a yarn/domain fibre volume fraction of 65%. At higher percentages, the fabric becomes too dense, impeding the impregnation of the polymer matrix during the manufacturing process. This results in the formation of dry pockets in the fabric, lacking the matrix, which significantly reduces the stiffness and toughness of the fabric [14].

3.2 TexGen and Voxel Mesh

The 3D composites required for FE analysis will be created using the software TexGen. TexGen is an open-source software licensed under the General Public License developed at the University of Nottingham for modelling textile structures. TexGen enables the creation of a wide variety of predefined textile structures, as well as the generation of custom structures through either the graphical user interface or the use of Python scripts. Figure 3.3 illustrates an example utilisation of TexGen in the creation of a 3D orthogonal non-woven fabric model.

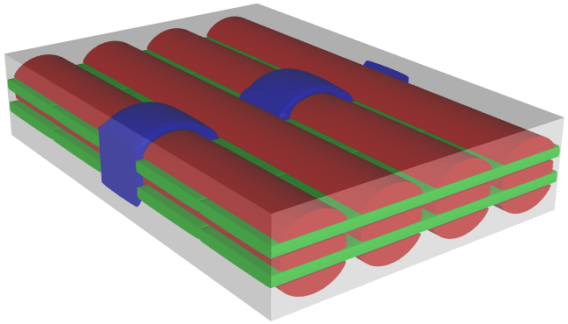

Figure 3.3: *3D orthogonal non-woven fabric.*

The textile can then be exported as a voxel mesh which can be imported into the FE software ABAQUS. A voxel mesh is a pixel-based mesh created by dividing the unit cell into a 3D grid of voxels, as in a grid of cubes [15]. This process, on an arbitrary textile, is illustrated in Figure 3.4.

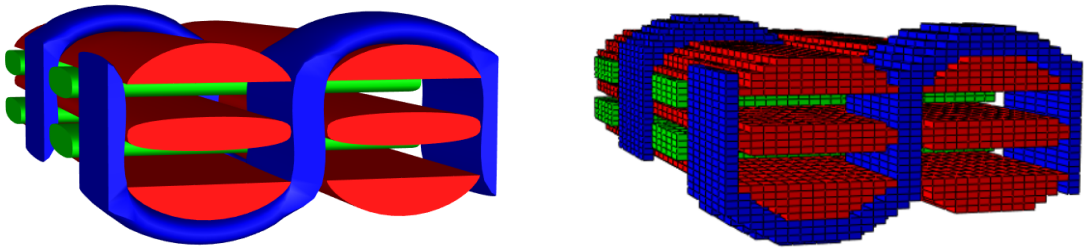

(a) *Textile in TexGen.*

(b) *Voxel mesh of yarns.*

Figure 3.4: *Dry Fibre (matrix/resin removed) voxel mesh.*

Composites have a periodic structure that can be described mathematically [16]. Therefore, applying voxel methods to composites creates a material resolution without changing the material properties. Voxel meshes are periodic by default, which is a necessity when periodic boundary conditions are going to be used. Figure 3.5 illustrates how a voxel mesh is applied to a unit cell boundary.

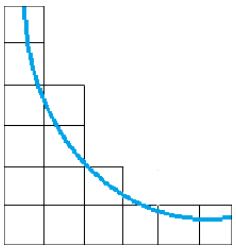

Figure 3.5: *Theoretical voxel mesh, where the blue line is the unit cell.*

Additionally, TexGen exports the element orientation of the mesh, which is utilised by ABAQUS to guarantee that the material properties for the yarns align with the local yarn directions. The element orientation is visualised in Figure 3.6 in the local coordinate system $[x, y, z]$ for the yarns. Note that for the through thickness yarns,

the local coordinate system will vary as the yarns oscillate between the layers, as illustrated with the two coordinate system axes for the through thickness yarn.

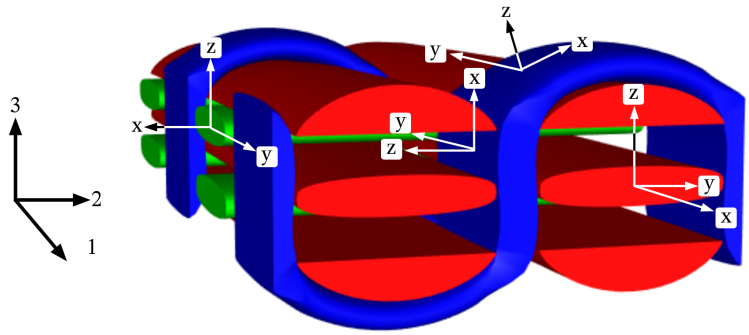

Figure 3.6: *Visualisation of element orientation in the local coordinate system* $[x, y, z]$.

3.3 Mechanical Analysis of 3D Orthogonal Non-Woven Fabrics

The mesoscale analysis is concerned with the non-woven material structure of the component. The main data inputs for this scale are the properties provided by the microscale, the homogeneous stiffness matrix of the yarn and the material properties for the matrix.

The textile models were generated using TexGen. Python scripts were developed and used to regulate and make minor adjustments to the textile models. Additionally, a Python script was created to calculate the approximate fibre distribution in the RVE. As a starting point, the aim was to create an RVE with a fibre distribution of 60% in direction *1*, 30% in direction *2* and 10% in direction *3*. The intention for all of the RVE models was to achieve a yarn fibre volume fraction of approximately 60% in each yarn and a domain fibre volume fraction of approximately 40-50% in the RVE.

Subsequently, the textile models were exported as voxel meshes and imported into ABAQUS. Prior to executing the easyPBC simulations in ABAQUS, it was necessary to modify the material properties for both the matrix and the yarns. Once more, TexGen was used, as it offers tools for calculating the fibre volume fractions of the yarns. Given that the yarns exhibit varying dimensions in the textile due to their interaction with each other, the yarns in direction *1*, yarns in direction *2* and through thickness yarns will also have distinct material parameters. These were extracted from the micro mechanical data sheet (Table 4.1) and utilised for the materials in ABAQUS.

The RVE models were then subjected to periodic boundary conditions using the EasyPBC plugin for ABAQUS to obtain the resulting orthotropic stiffness matrix. Furthermore, these obtained orthotropic elastic stiffness properties were used as inputs for the macroscale simulations. The results were evaluated and utilised as an indication of how the RVE needed to be modified to strengthen the material to improve the failure criteria. This method was iterated several times until a

sufficiently strong material was obtained.

Furthermore a convergence analysis was carried out. The convergence analysis was carried out on an RVE using 10, 20, 30, 40, 50 and 60 voxel counts in every direction. The size of the voxels is dependent on the size of the RVE; however, as the size of the RVE is approximately consistent between the models, the size of the voxels will also be approximately consistent.

Additionally, an analytical validation was conducted to ensure the accuracy of the FE simulations of the RVE in comparison to the analytical solution. The analytical solution was calculated using the mixed iso-stress and iso-strain model presented in Section 3.3.1.

3.3.1 Analytical Modelling of Mechanical Elastic Properties in Composite Materials

In order to analytically verify the mechanical elastic properties on the mesoscale, an analytical modelling scheme was used. The *Mixed Iso-Stress* and *Mixed Iso-Strain* based unit cell modelling scheme was utilised as it can be used to predict the elastic mechanical properties for 3D orthogonal non-woven composite materials [17].

By considering a piece of material at the mesoscale from a 3D orthogonal non-woven composite, see Figure 3.7a, where the three yarn groups of assumed rectangular cross-sectional area are placed in the orthogonal directions in the coordinate system [*1*, *2*, *3*], the marked volume (in grey) can be treated as a unit cell (shown in Figure 3.7b).

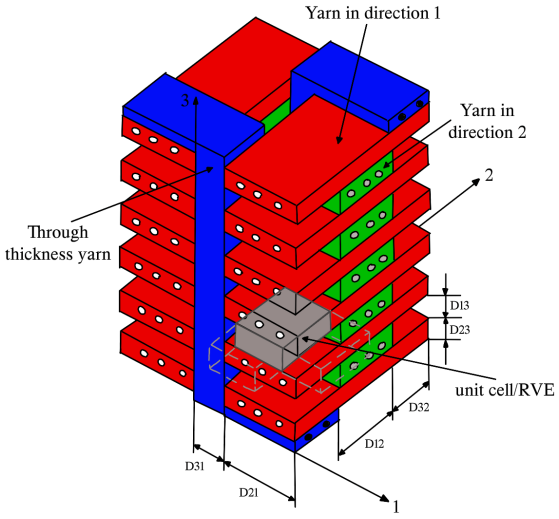

(a) *3D orthogonal non-woven composite.*

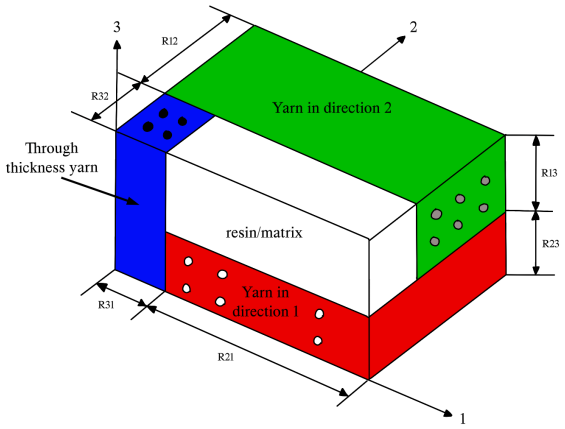

(b) *Unit cell/RVE.*

Figure 3.7: *3D orthogonal non-woven composite and RVE, inspiration taken from [6].*

The elastic properties for the RVE can be obtained analytically using the method presented in Appendix A.2. The analytically computed elastic properties can act as a benchmark and point of validation for the properties computed using more advanced computational FE models presented in the following sections.

3.3.1.1 Analytical Validation

The analytical validation results are presented in Table 3.1, describing the values for the analytical solution and the RVE model in Figure 3.8.

Table 3.1: Comparison between analytical solution and RVE solution.

	Analytical	RVE
$V_{f,d}$ [%]	45.0	43.0
E_1 [GPa]	66.4	64.7
E_2 [GPa]	44.9	44.2
E_3 [GPa]	25.1	20.7
G_{12} [GPa]	3.6	4.5
G_{23} [GPa]	4.1	3.6
G_{31} [GPa]	4.1	3.8
ν_{12}	0.084	0.093
ν_{13}	0.182	0.193
ν_{23}	0.178	0.194

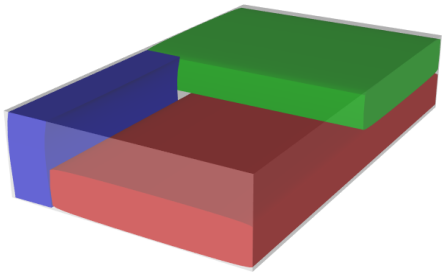

Figure 3.8: *RVE used for the analytical validation.*

A review of the data presented in Table 3.1 reveals a significant observation: the RVE model consistently generates results that align closely with the analytical solution. The comparison reveals a mere 10.6% deviation on average between the outcomes obtained from the RVE model and those derived analytically.

This precision shows the reliability of the FE models in capturing the complexity of the RVEs. It can be concluded from these findings that the FE approximations yield outcomes that are in close accord with the calculated analytical solution. Consequently, the FE models were found to be reliable and will subsequently be adopted for further analysis in this study.

3.3.2 Results – Simulated Yarn Architectures

The RVE models and their respective coordinate systems, Figure 3.10 a-f, are oriented along the OGV in accordance with Figure 3.9. For each simulated RVE, the fibre distribution (FD), the domain fibre volume fraction ($V_{f,d}$), the failure criteria (FC) from the macroscale and the resulting orthotropic stiffness properties are presented in Table 3.2.

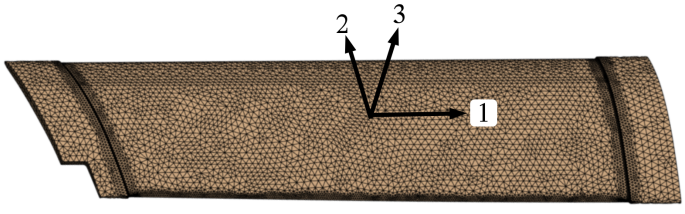

Figure 3.9: *Visualisation of orthogonal mesoscale fibre distribution on the OGV.*

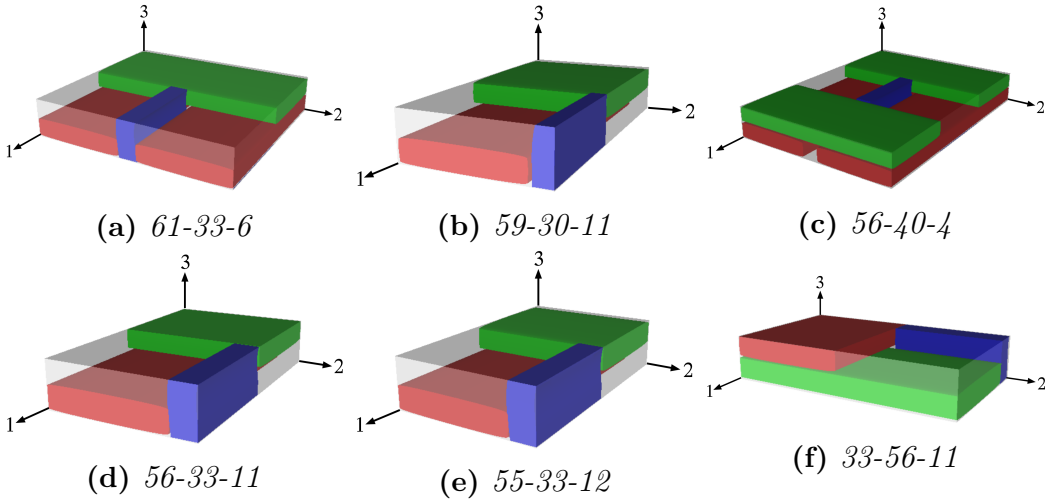

(a) *61-33-6* **(b)** *59-30-11* **(c)** *56-40-4*

(d) *56-33-11* **(e)** *55-33-12* **(f)** *33-56-11*

Figure 3.10: *Simulated yarn architectures with fibre distribution [%] in the [1, 2, 3] directions. For example, "56-33-11" has the fibre distribution 56% in direction 1, 33% in direction 2 and 11% in direction 3.*

Table 3.2: Data for the simulated yarn architectures.

	Material					
	"61-33-6"	"59-30-11"	"56-40-4"	"56-33-11"	"55-33-12"	"33-56-11"
FD_1 [%]	60.7	59.0	55.7	55.9	55.0	33.1
FD_2 [%]	33.0	30.3	40.4	33.1	32.9	55.9
FD_3 [%]	6.3	10.7	3.9	11.0	12.1	11.0
$V_{f,d}$ [%]	43.4	41.1	47.5	45.6	45.6	45.6
E_1 [GPa]	69.7	64.9	70.5	68.5	68.1	42.4
E_2 [GPa]	44.3	39.1	54.7	42.4	46.3	68.5
E_3 [GPa]	16.6	15.5	16.3	21.1	22.5	21.1
G_{12} [GPa]	4.6	3.9	4.9	4.6	5.1	4.6
G_{23} [GPa]	3.7	3.2	4.1	3.7	4.0	3.8
G_{31} [GPa]	3.6	3.3	4.0	3.3	4.1	3.7
ν_{12}	0.090	0.090	0.076	0.099	0.098	0.061
ν_{13}	0.240	0.235	0.269	0.193	0.192	0.193
ν_{23}	0.244	0.230	0.270	0.194	0.193	0.194
FC	1.161	1.262	1.143	1.143	1.126	1.699

3.3.2.1 Discussion – Simulated Yarn Architectures

Table 3.2 indicates that the material denoted "55-33-12" most closely meets the failure criteria. This material is among the materials that has the highest domain fibre volume fraction and the highest shear stiffness of all the investigated materials.

Furthermore, "33-55-11" is the only material that has the majority of the fibre distribution in direction *2*. However, it is important to note that this material has

the same domain fibre volume fraction as "55-33-11". Since the failure criteria for "33-55-11" significantly exceed those for the other materials, it was concluded that, considering the load case on the OGV, it is crucial for the majority of the fibre distribution to align along direction *1*.

The materials "56-33-11" and "59-30-11" exhibit different domain fibre volume fractions and therefore different values of the failure criteria. "56-33-11" has the highest domain fibre volume fraction of them both and thus have a lower value of the failure criteria. Whereas, "59-30-11" has a lower domain fibre volume fraction, which consequently leads to a higher value of the failure criteria.

These results indicate that the domain fibre volume fraction is a key factor in determining whether a material meets the failure criteria. As previously stated in Section 2.1, the materials should have a failure criteria of around 1 in order to be deemed viable. This implies that a lower domain fibre volume fraction will result in exceeding the failure criteria, rendering the material unsuitable for use on the macroscale.

One should also note that the model geometry created in TexGen is a highly idealised representation of a 3D orthogonal non-woven fabric. This means that local variations or misalignment's in the fibre distribution are not accounted for. In a realistic textile the top and bottom through thickness yarns would contribute to lowering the domain fibre volume fraction. This is further developed in Section 3.3.3.

3.3.3 Comparison between RVE and Textile

A comparison between the obtained mechanical elastic properties for FE simulations on the RVE in Figure 3.11a and the textile in Figure 3.11b are presented in Table 3.3.

Table 3.3: Comparison between RVE FE solution and textile FE solution.

	RVE	Textile
$V_{f,d}$ [%]	43.0	35.2
E_1 [GPa]	64.7	52.0
E_2 [GPa]	44.2	28.0
E_3 [GPa]	20.7	8.8
G_{12} [GPa]	4.5	3.6
G_{23} [GPa]	3.6	2.8
G_{31} [GPa]	3.8	2.8
ν_{12}	0.093	0.092
ν_{13}	0.193	0.309
ν_{23}	0.194	0.403

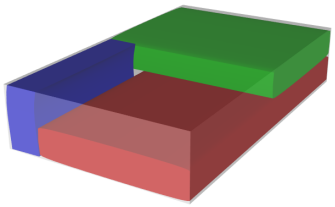

(a) *RVE.*

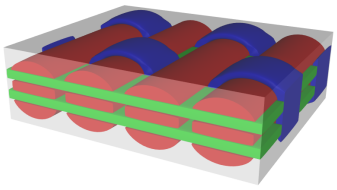

(b) *Textile.*

Figure 3.11: *RVE and textile used in the comparison between RVE and Textile models.*

As seen in Table 3.3, the discrepancy between the RVE and the textile models is considerably pronounced, with an average difference of 39.1%. This is due to the surface properties caused by the top and bottom of the through thickness reinforcements which will further be discussed in Section 3.3.3.1.

3.3.3.1 Influence of the Top and Bottom Through Thickness Yarns for the Stiffness of the Material

It is evident that the engineering constants for the RVE and the textile model in Table 3.1 differ significantly. The structure of the through thickness yarns results in the larger textile having a substantially lower domain fibre volume fraction (approximately 35%) compared to the cut-out RVE from the same textile (approximately 43%), as illustrated in 3.12.

This is a consequence of the through thickness yarns that runs over the yarns in direction *1*, which adds height to the textile domain (see Figure 3.12b). The increased height will contribute to a higher volume, which will increase the amount of matrix in the RVE, and thus decrease the strength of the textile. This is due to the fact that the quantity of matrix affects the characteristics of the RVE. Consequently, an increase in the quantity of matrix results in a reduction in the strength of the RVE.

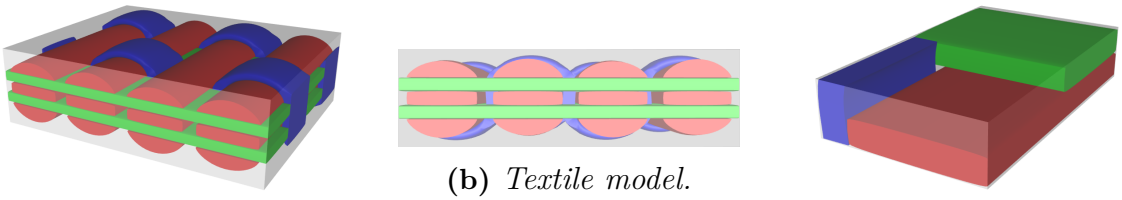

(a) *Textile model.* **(b)** *Textile model.* **(c)** *RVE.*

Figure 3.12: *Textile model with a domain fibre volume fraction of approximately 35% and RVE with a domain fibre volume fraction of approximately 43%.*

However, this has a much greater influence on the stiffness for thinner textiles. For thicker textiles, such as in Figure 3.13, the added volume is smaller in relation to the volume of the textile and therefore the effect is not as substantial, which can be seen in Table 3.4.

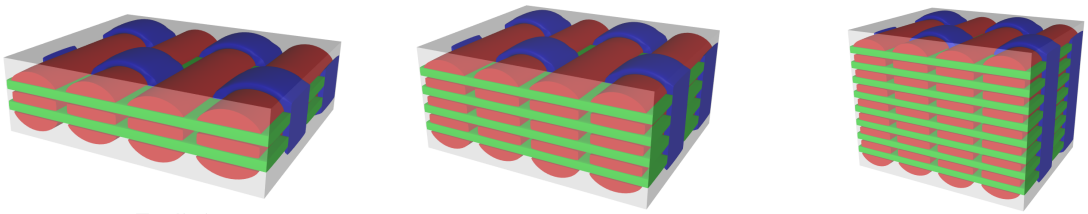

(a) $V_{f,d} \approx 35\%$, *Thickness* $\approx 2.8mm$. **(b)** $V_{f,d} \approx 38\%$, *Thickness* $\approx 4.4mm$. **(c)** $V_{f,d} \approx 40\%$, *Thickness* $\approx 7.6mm$.

Figure 3.13: *Increasingly thick textile models.*

Table 3.4: Engineering constants for the RVE and textile model in Figure 3.12 and for increasingly thicker textiles as in Figure 3.13.

	RVE	Textile 1	Textile 2	Textile 3
$V_{f,d}$ [%]	43.0	35.2	37.9	39.9
E_1 [GPa]	64.7	52.0	52.4	59.7
E_2 [GPa]	44.2	28.0	35.1	36.1
E_3 [GPa]	20.7	8.8	10.7	13.3
G_{12} [GPa]	4.5	3.6	3.8	4.0
G_{23} [GPa]	3.6	2.8	3.0	3.2
G_{31} [GPa]	3.8	2.8	3.0	3.3
ν_{12}	0.093	0.092	0.083	0.093
ν_{13}	0.193	0.309	0.276	0.243
ν_{23}	0.194	0.403	0.354	0.288

However, in practice, the quantity of additional matrix would not be as substantial as it is in these approximate textile models. During the manufacturing process and the impregnation of the textile, the yarns would interact with each other and the curves in the through thickness yarns would be squeezed and flattened, resulting in less additional matrix. This in turn, would lower the weakening effect of the added matrix.

When extracting an RVE, in order to analyse the elastic properties for a 3D orthogonal non-woven textile, it is important to note how the thickness affects the data. Due to the time constraints of this thesis and the fact that the OGV is considerably thicker than the simulated textile model, further investigations into this matter is not feasible. Consequently, the RVE approximation was employed.

3.4 Analysis of how 45° Yarn Layers affect the Stiffness of the Textile

Textile models with 45° yarn layers were also modelled and simulated in order to investigate the influence of these layers on the stiffness of the textile. This was done to validate the hypothesis that 45° yarn layers in the textile will increase the shear moduli, which could be beneficial given the load conditions on the OGV. The models were created by adding one +45° yarn layer and a -45° yarn layer on top of each other in the middle of the textile.

3.4.1 Results – Textile with 45° Yarn Layers

Figure 3.14 shows the simulated 45° yarn layer RVE and Table 3.5 shows the results for the simulation along with the failure criteria from the macroscale.

Table 3.5: Results for textile model with 45° yarn layers.

	45° RVE
$V_{f,d}$ [%]	42.0
E_1 [GPa]	59.5
E_2 [GPa]	43.1
E_3 [GPa]	20.7
G_{12} [GPa]	4.2
G_{23} [GPa]	3.5
G_{31} [GPa]	3.5
ν_{12}	0.095
ν_{13}	0.187
ν_{23}	0.186
FC	1.307

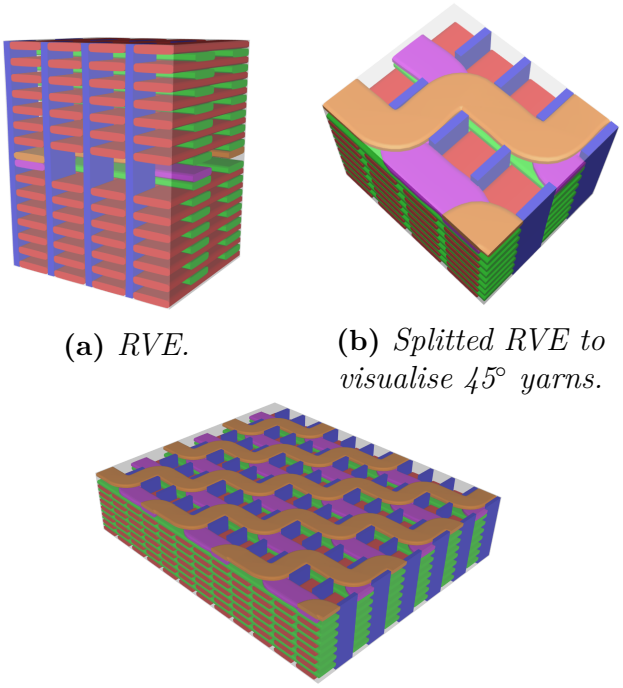

(a) *RVE.*

(b) *Splitted RVE to visualise 45° yarns.*

(c) *Repeated splitted RVE to visualise 45° yarn pattern.*

Figure 3.14: *Textile model with 45° yarn layers.*

3.4.1.1 Discussion – Textile with 45° Yarn Layers

As seen in Table 3.5, the textile with the 45° yarn layers does exceed the failure criteria. The hypothesis was that the 45° yarn layers would increase the shear moduli of the material. However, the limited results do not permit this conclusion to be drawn. This suggests that further investigations and simulations are required in order to draw any conclusions about the influence of the 45° yarns on the shear moduli in the material. Due to the time constraints of this thesis, such considerations are not feasible.

It is worth noting that the 45° yarns, as seen in Figure 3.14b, add a relatively large amount of matrix to the domain. This results in a reduction of the domain fibre volume fraction in the textile, which in turn weakens the material properties. However, the geometry used for the 45° textile is idealised and the real material would not behave in the same way. This is mainly due to the fact that the yarns interact with each other during the manufacturing process; the yarns move around, push each other around and the shape of the yarns therefore changes. Additionally, the yarns would be subject to the influence of gravity, which would cause them to "drop" into the matrix pockets, resulting in a curved path through multiple planes. The yarns would therefore not lie in a single plane as depicted in Figure 3.14, but rather in multiple planes. This would allow for tighter packing of the textile which would reduce the size of the resin pockets, consequently decreasing the weakening

effect.

In addition, the 45° yarns would not "snake" their way through the material in a realistic textile. Rather, they would interact with the through thickness yarns, displace them and follow a more straight path. The representation of the off-axis yarns in this manner is primarily a consequence of the constraints imposed by TexGen, which currently lacks the capability for a more accurate depiction. Furthermore, our current comprehension and knowledge of TexGen also contribute to this non-realistic modelling.

Given these factors, the geometry of the 45° fabric likely differs significantly from that of a realistic fabric. Consequently, the approximations are also likely to be less accurate. It has been demonstrated that 45° yarns in unidirectional carbon fibre laminates enhance the shear stiffness moduli, and this phenomenon should be applicable to 3D orthogonal non-woven fabrics as well.

However, off-axis yarns in 3D orthogonal non-woven fabrics are a relatively new field of research, and as a result, there is still much uncertainty regarding the most appropriate methods for analysing them [14].

3.5 Sources of Error

The material properties evaluated in the macroscale model were based solely on the RVE, thus the impact if the through thickness yarns was not modelled in the macroscale FE model. The near net-shaped Noobed 3D pre-forms still exhibit through thickness yarns along the surface of the pre-form. This would impact the stiffness of the material in regions of thin sections and the effects of the through thickness yarns were presented in Chapter 3.3.3.1. The thin edges of the OGV would be an area where the effect would be exacerbated. The area which is under the largest strain in the OGV model is also an area which would be affected by the softening derived from the increase in the proportion of through thickness yarns in the textile.

The model geometry considers idealised or close-to-idealised geometries in the yarn architecture. It is therefore important to note that the yarns will not be perfect rectangles; they can also be circular or a mixture of both. Moreover, this is not what a common yarn structure looks like, as mentioned in Section 3.1. However, no experiments or CT scans have been conducted in this thesis, and the geometry of the yarn architecture and cross section applied is therefore only a guess.

4
Microscale

The microscale, the smallest scale of our examination, supplies the mesoscale with precise yarn material properties for simulations, which are then validated at the macroscale. Various methods for calculating elastic and thermal properties are discussed in this section. These include simulations and analytical solutions, where the analytical solutions are implemented in order to validate the results from the FE simulations. Due to the inclusion of both mechanical and thermal analysis, the microscale study is divided into two sections. Each section outlines the methodologies and theories applied, followed by a discussion of the results. The microscale uses the $[x, y, z]$ coordinate system, with the fibres aligned along the x-direction.

4.1 Mechanical Analysis

To calculate the mechanical properties of the microscale, ANSYS Material Designer Toolbox was utilised. This toolbox randomly generates a unidirectional microscale RVE consisting of the two constituent materials (carbon fibre and epoxy) given a specific fibre volume fraction. This was simulated using 0 degree in mean misalignment angle of the carbon fibres inside the microscale RVE.

The simulation was carried out for different volume fractions ranging from 35% to 65% in increments of 5%. This allows for the interpolation of specific mechanical properties within this range, which is essential for the mesoscale analysis. To verify the effect of different RVE sizes a convergence analysis was conducted. The RVE is modelled using a periodic mesh with PBCs. The acquired material properties are presented in Section 1.2.3. The calculated results will be compared with available analytical solutions presented in the following sections.

4.1.1 Longitudinal and Transverse Properties Using the Voigt-Reuss Method

To verify the outcome of elastic material properties, analytical methods can be employed. These methods utilise the respective volume fractions of the constituents to create a weighted mean of the matrix and carbon fibre elastic properties, resulting in a system's total Young's modulus E_{xx} and E_{yy}. By approximating the micromodels constituent materials as springs either parallel *(Voigt)*, or coupled in series *(Reuss)*, one can find the analytical solution to Young's modulus along the fibre and transverse to the fibre, as outlined in [18]. This will thus provide an upper and lower bound for the elastic modulus, with the actual value lying somewhere between these

two extremes.

The modulus of the fibre and matrix materials are denoted by E_f and E_m, respectively, where the subscripts f and m correspond to fibre and matrix. The volume fractions of these materials, V_f and V_m, satisfy the condition $V_f + V_m = 1$.

Consider first the case of the Voigt assumption. As seen in figure 4.1 a total axial stress σ_{ax} is applied following the fibre direction. The stress is equal to the sum of stresses in fibres σ_f and matrix σ_m and results in a strain ε_x. Here it is assumed that the axial force creates a strain in direction x that is equal everywhere in the RVE since no slip condition between the fibres and matrix exist. Therefore, the elastic properties in the fibre direction can be written as,

$$E_{xx} = \frac{A_f}{A}E_f + \frac{A_m}{A}E_m = V_f E_f + V_m E_m, \tag{4.1}$$

according to [18].

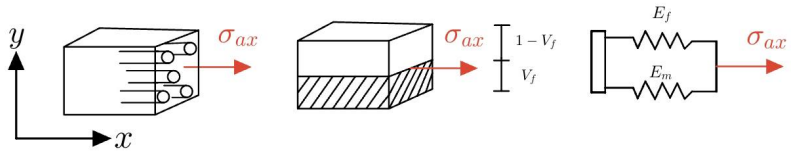

Figure 4.1: *Voigt material idealisation.*

Using the same notation as above but now applying a axial stress cross fibre direction σ_{ay} that can be assumed to impose a stress equal in each material. The cross fibre directional elastic stiffness can be written as,

$$E_{yy} = \frac{E_f E_m}{V_f E_m + V_m E_f}. \tag{4.2}$$

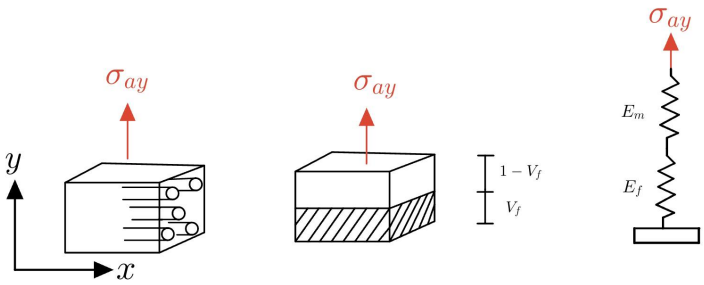

Figure 4.2: *Reuss material idealisation.*

4.1.2 Analytical Shear Modulus

Furthermore, [18] suggest an analytical method for calculating the lower bound of the shear modulus G_{xy}. Assuming that a shear stress τ_{xy} is applied to the micro model. Denoting the shear modulus with G_f and G_m respectively, the shear stress will result in a shear both in the fibre material and matrix,

$$\gamma_f = \frac{\tau_{xy}}{G_f} \tag{4.3}$$

$$\gamma_m = \frac{\tau_{xy}}{G_m}. \tag{4.4}$$

By analysing Figure 4.3, the resulting displacement δ_{xy} can be calculated using each shear and volume fraction V_f and V_m where L denotes the entire length in the y-direction.

$$\delta_{xy} = L(V_f\gamma_f + V_m\gamma_m). \tag{4.5}$$

The resulting shear modulus G_{xy} can therefore be defined as

$$\gamma_{xy} = \frac{\delta_{xy}}{L} = \frac{\tau_{xy}}{G_{xy}}. \tag{4.6}$$

Using Eq. (4.3 - 4.4), G_{xy} can be written as

$$G_{xy} = \frac{G_f G_m}{V_f G_m + V_m G_f}. \tag{4.7}$$

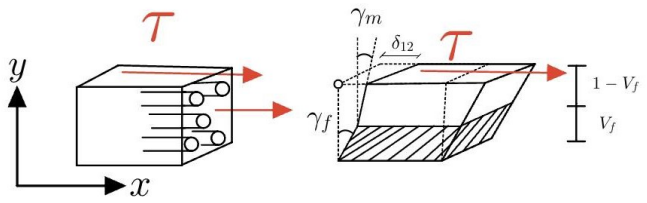

Figure 4.3: *Analytical shear model.*

4.1.3 Microscale Mechanical Results and Discussion

The result of the calculated micromechanical properties are presented in Table 4.1. The simulation was conducted using the specified fibre diameter of 7 μm provided by Fureho AB and the elastic properties presented in Table 1.1 for the fibres and epoxy.

Table 4.1: Elastic Properties and Poisson's ratios for microscale.

Fraction [%]	35	40	45	50	55	60	65
E_{xx} [GPa]	86.19	98.025	109.85	121.68	133.49	145.30	153.92
E_{yy} [GPa]	6.94	7.67	8.59	10.10	13.20	15.30	18.60
E_{zz} [GPa]	7.03	7.88	9.03	10.55	13.00	15.30	17.90
G_{xy} [GPa]	2.79	3.14	3.57	4.18	5.50	6.32	7.72
G_{yz} [GPa]	2.55	2.91	3.32	3.84	4.39	5.14	6.16
G_{zx} [GPa]	2.81	3.24	3.78	4.44	5.32	6.31	7.49
ν_{xy}	0.304	0.305	0.305	0.306	0.307	0.307	0.308
ν_{xz}	0.305	0.305	0.306	0.306	0.307	0.307	0.308
ν_{yz}	0.383	0.379	0.369	0.354	0.324	0.321	0.316

Table 4.1 confirms that the microscale exhibits transversely isotropic behaviour, as indicated in Table 1.2. Figures 4.4a-4.4b showcase where the points are relative to the analytical solution. The shaded grey area in Figure 4.4a represents the region between the analytical upper and lower bounds of E. It can be seen that ANSYS Material Designer gives a valid result within the bounds of the analytical solution for the elastic properties E_{xx}, E_{yy} and G_{xy}.

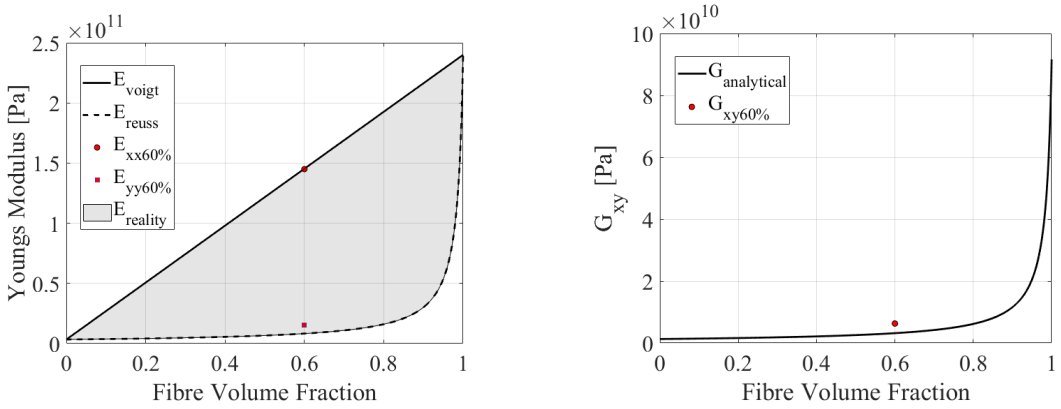

(a) *Analytical solution for E_{xx}, E_{yy}.* **(b)** *Analytical solution for G_{xy}.*

Figure 4.4: *Analytical and simulated E_{xx}, E_{yy} and G_{xy} for 60 [%] fibre volume fraction.*

4.2 Thermal Analysis

The objectives of the thermal analysis were twofold: firstly, to acquire the transversely isotropic conductivity of the composite material, and secondly, to predict the effect of heat transfer across the OGV when a thermal element was embedded into the material.

The thermal conductivities were extracted using ANSYS Material Designer, with a similar model to the one used in the mechanical analysis. Five simulations were carried out for each volume fractions ranging from 40% to 65% in increments of 5%. The average result of these five simulations was calculated for each specific volume fraction. Due to the transversely isotropic material properties, which are isotropic in directions perpendicular to the fibre direction, an error in thermal conductivity of less than 3% between the y- and z-directions was deemed acceptable. This error rate also serves as a good indicator of model convergence, since in the ideal case these values would be identical. All simulations were run implementing a conformal and periodic mesh and solved with respect to PBCs. The simulated conductivities are then compared with analytically obtained conductivity values.

To evaluate heat transfer across the OGV, a micro-thermal model was established using the ANSYS Transient Thermal workbench. This model, intended to represent a small repeating section of the OGV's surface, incorporated a thermal element embedded in the composite, utilising previously simulated conductivities as material parameters. As shown in Figure 4.5, the model featured a convective boundary condition on one edge to simulate the impact of outdoor conditions, while the remaining three edges were insulated to reflect the symmetry of the repeated section. Additionally, a predetermined temperature from the thermal element was applied in the simulations.

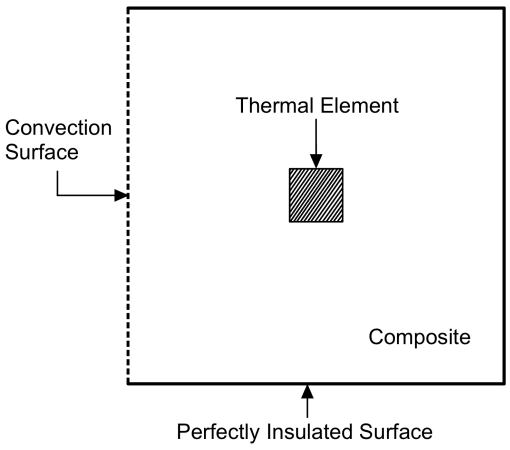

(a) *Model overview.*

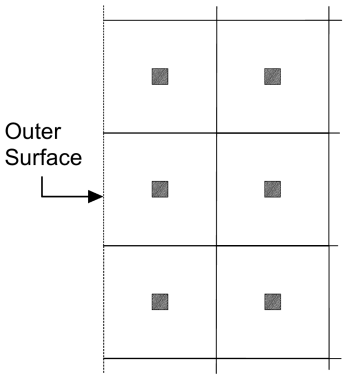

(b) *Displays symmetry and position of model within OGV.*

Figure 4.5: *Illustration of the model used for the heat transfer simulations and corresponding boundary conditions.*

4.2.1 Analytical Thermal Conductivity with Lewis-Nielsen Model

To validate the thermal conductivity coefficients obtained through FE simulations and presented in the following section, an analytical approach is employed for comparison. Among the methods for predicting the conductivity of composite materials, the Lewis-Nielsen model has been identified as the most accurate, particularly up to a fibre volume fraction of 0.51 [19]. Therefore, it will be utilised as the benchmark model for verifying the results.

The Lewis-Nielsen model consists of a set of equations given by

$$\frac{k}{k_m} = \frac{1 + ABV_f}{1 - \psi BV_f}, \tag{4.8}$$

$$A = K_E - 1, \tag{4.9}$$

$$B = \frac{k_f/k_m - 1}{k_f/k_m + A}, \tag{4.10}$$

$$\psi = 1 + \left(\frac{1 - \phi_{max}}{\phi_{max}^2}\right) V_f. \tag{4.11}$$

The thermal conductivity, k, of the composite material in directions perpendicular to fibres can be evaluated from Eq. (4.8). Constants A, K_E, and ϕ_{max} relate to the shapes, packing, and orientation of the fibres within the matrix. Detailed definitions and applications of these constants can be found in the Lewis-Nielsen model [20].

For conductivity in the direction parallel to the fibres, the rule of mixtures, Eq. (4.12), can be utilised

$$k = k_f V_f + k_m V_m, \tag{4.12}$$

which is a valid approximation when the ratio of fibre length to diameter is $\gg 1$ [20]. The conductivity values for the individual fibres and matrix are given in Table 1.1.

4.2.2 Results and Discussion of Simulated Thermal Conductivity Values

The thermal conductivities of the composite for varying volume fractions and fibre directions are presented in Table 4.2. The discrepancies between analytically obtained values and values obtained from ANSYS Material Designer are presented in Figure 4.6.

Table 4.2: Thermal conductivities in directions parallel (k_x) and perpendicular ($k_y = k_z$) to fibres.

Fraction [%]	k_x [W/mK]	k_y [W/mK]
40	3.96	0.48
45	4.43	0.56
50	4.90	0.66
55	5.37	0.78
60	5.84	0.94
65	6.13	1.05

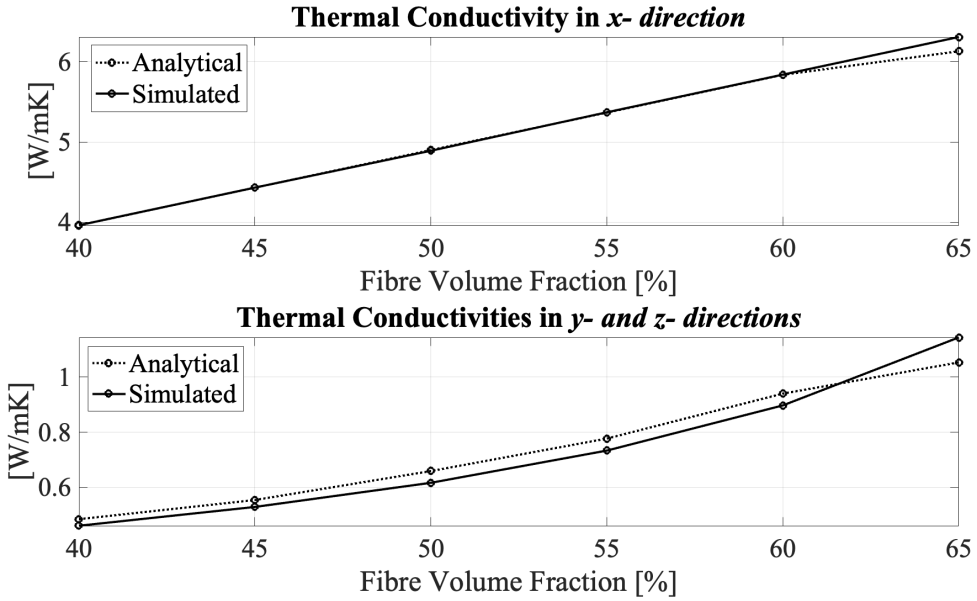

Figure 4.6: *Simulated vs analytical conductivities in directions parallel (x) and perpendicular (y,z) to fibres.*

As seen in Table 4.2, the thermal conductivity in the *x-*,*y-* and *z-* directions increases with increasing fibre volume fraction, in accordance with the analytical solution. After reaching approximately 60% fibre volume fraction, the simulated thermal conductivity surpassed that of the analytical solution. This indicates uncertainty and reinforces the expectation from the analytical model, which stands as most accurate for lower fibre volume fractions [20]. Nevertheless, the values are closely aligned, suggesting that the model has successfully predicted the thermal conductivities.

Based on the results, it is evident that the fibres exhibit superior heat conductivity compared to the matrix. This accounts for the higher conductivity observed in the direction parallel to the fibres compared to the perpendicular directions. Furthermore, the increase in fibre content correlates with the rise in conductivity.

4.2.3 Transient Thermal Analysis

The Transient Thermal Analysis workbench in ANSYS is used to model the temperature and heat flux over a small section at the surface of the OGV. The governing equation is the *heat diffusion equation* [21]. For a transversely isotropic material, where the material properties are equal in the transverse and out-of-plane directions, the equation, without internal heat source, becomes

$$\frac{\partial}{\partial x}\left(k_x \frac{\partial T}{\partial x}\right) + \frac{\partial}{\partial y}\left(k_y \frac{\partial T}{\partial y}\right) + \frac{\partial}{\partial z}\left(k_y \frac{\partial T}{\partial z}\right) = \rho c_p \frac{\partial T}{\partial t}, \tag{4.13}$$

where k is the thermal conductivity of the solid material, which remains the same in the out-of-plane directions, y and z. In a composite material comprising of two distinct components, the density, ρ, and specific heat, c_p, can be determined using the rule of mixtures, stated as

$$\begin{aligned} \rho &= V_f \rho_f + V_m \rho_m, \\ c_p &= V_f c_{p,f} + V_m c_{p,m}. \end{aligned} \tag{4.14}$$

An essential factor required for modelling the influence of airflow over the surface is the average convection coefficient $\overline{h}$. To estimate it we can approximate the OGV as a flat plate and utilise theory developed for flat plates in parallel flow [21]. Assuming laminar flow, the following relation holds for the average Nusselt number

$$\overline{Nu_L} \equiv \frac{\overline{h_L} L}{k} = 0.664 Re^{1/2} Pr^{1/3}. \tag{4.15}$$

The air properties, k and Pr, are evaluated at the relevant ambient temperature. Using Eq. (4.15), the average convection coefficient on the surface of the model can be calculated.

The simulations that produced the results discussed in the following section utilised a convection coefficient of 35 W/m^{2}K. This coefficient is based on an ambient temperature of -10 °C and a wind speed of 10 m/s. Additionally, a predetermined temperature from the thermal element was applied in the simulations. The density and specific heat values for the individual fibres and matrix are given in Table 1.1.

4.2.4 Results and Discussion of Heat Transfer Simulation using ANSYS

The results of the heat transfer analysis on the OGV are summarised in Table 4.3. Key findings include measurements of surface temperatures on the OGV and the maximum heat flux throughout the model for various fibre volume fractions. In addition, the total time for steady state convergence is estimated.

Table 4.3: Thermal properties for varying fibre volume fractions.

Fraction [%]	Steady State Surface Temperature [°C]	Maximum Heat Flux [W/m³]	Convergence Time [s]
40	53.3	8791.0	820
45	53.3	8791.5	815
50	53.4	8791.8	800
55	53.4	8792.0	790
60	53.4	8791.9	770
65	53.4	8792.0	750

Figure 4.7 shows the result of the temperature simulation for a fibre volume fraction of 50%. The internal temperature of the thermal element is consistently maintained at approximately 60 °C across all volume fractions. Figure 4.8 illustrates the temperature distribution across increasing time steps. Subfigures (a) to (f) show the progression from the initial state before the thermal element is engaged to 10 minutes afterwards, at various intervals.

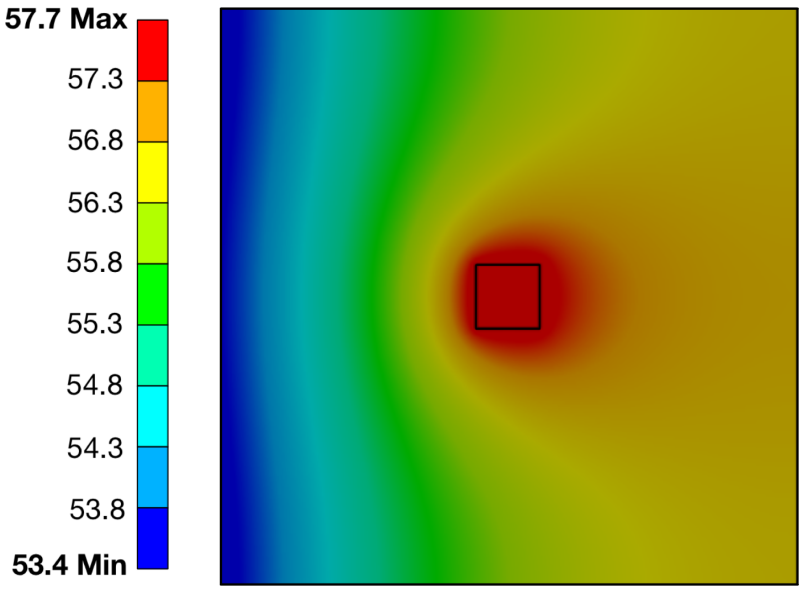

Figure 4.7: *Temperature distribution* [°C] *for 50% fibre volume fraction over a simulation period of 1000 seconds.*

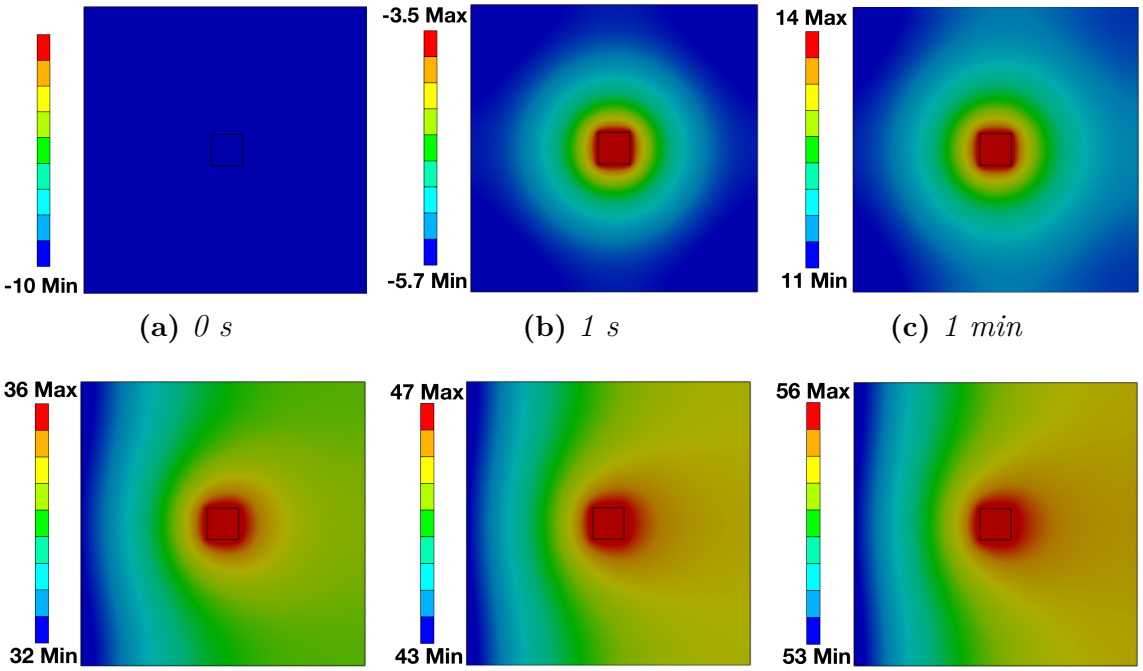

(a) *0 s* **(b)** *1 s* **(c)** *1 min*

(d) *3 min* **(e)** *5 min* **(f)** *10 min*

Figure 4.8: *Temperature distribution* [°C] *across increasing time steps.*

The data presented in Table 4.3 demonstrates minimal variation in values across different fibre reinforcements. Thus, the temperature distributions for each fibre volume fractions closely resemble those shown in Figure 4.7.

The maximum temperature and heat flux are observed at the thermal element, whereas the minimum temperature occurs at the OGV surface, which is expected due to convection there. Figure 4.8 demonstrates that the temperature in the model rises rapidly initially, then stabilises to a steady state shortly after 10 minutes.

No analytical method for predicting the heat flux or temperature distributions has been used to verify the results of the simulations. Therefore, future work should include the development and application of analytical benchmarks or experimental testing to validate the findings and ensure their accuracy.

4.3 Sources of Error

The homogenised mechanical and thermal properties were predicted using ANSYS Material Designer, which allows the user to specify a repeating count (RPC). A higher RPC allows for a larger microscale model that contains more fibres which make the model more accurate and representative, especially when the fibres are randomly distributed. The RVE size with a RPC 7 corresponds to an area of roughly 1900μm and a length of 120μm. However, this also raises the demands on the computer's CPU. In this study, an RPC of 7 was chosen because the available computers could not deliver results in a reasonable timeframe for larger RPCs. Nonetheless, a convergence study confirmed that an RPC of 7 was sufficient to achieve accurate results.

It should be mentioned that the results achieved for the micro mechanical properties are based on only one randomly generated RVE and that the results may vary under a different configuration. This due to the fact that the carbon fibre distance to the outer wall and its relative distances, which are randomly configured, influence the RVE stiffness. For future work one might consider taking an average over several randomly generated RVE's for a more representative result.

5
Conclusion

The conclusions drawn throughout this Bachelor Thesis are presented below. They are presented in the same order as the chapters in this thesis; macroscale, mesoscale and microscale. The conclusions are directly associated to the goals presented in Section 1.3.1.

Macroscale

An FE model was developed of the OGV in ANSYS Mechanical to validate the mechanical elastic properties of the 3D orthogonal non-woven composite. Element orientation was included in the model to more accurately represent the directional properties of the material in the vane. A strain-based FC was formulated and it utilised the element orientation to evaluate the strain in each elements local coordinate system. Using this macroscale model it was possible to propose a set of elastic stiffness properties that can be used to inform GKN and Fureho when they select a final yarn distribution and architecture for their component.

Mesoscale

A working analysis method for obtaining the mechanical elastic properties of a designed 3D orthogonal non-woven composite was developed. Furthermore, a periodic mesh was created using voxels to facilitate the use of the ABAQUS plugin EasyPBC.

The majority of the yarn architecture presented in Table 3.2 are suitable for the OGV, as their failure criteria are around 1. One of these materials are "55-33-12", which also has the highest domain fibre volume fraction. The domain fibre volume fraction turned out to be a key factor for the stiffness of the textile, and plays a role in determining whether a material is close to fulfilling the failure criteria.

However, due to the factors contributing to uncertainties in the results discussed in the previous chapters, further investigations and experimental tests need to be carried out before one could make any confident decisions about the yarn architecture. The results in Section 3.3.2 should be viewed as theoretical material parameters for the textiles which can be used as a starting point for further investigations.

It is crucial to acknowledge that the top and bottom of the through thickness reinforcements exert a significant influence on the stiffness of the textile, as they affect the domain fibre volume fraction. This phenomenon is particularly pronounced in thinner textiles, where the increased volume is proportionately greater. As the thickness of the textile increases, the effect becomes less pronounced, and the elastic properties approach those of the RVE.

It is also important to note that the hypothesis with 45° yarn layers and how its structure can effect the shear stiffness modulus could not be confirmed. As stated earlier, it has been demonstrated that 45° yarns in unidirectional carbon fibre laminates enhance the shear stiffness moduli, and this phenomenon should be applicable to 3D orthogonal non-woven fabrics as well.

Microscale

An analysis tool for extracting elastic mechanical and thermal properties on the microscale using FE models of RVE's was developed through the use of ANSYS Material Designer. In order to ensure the accuracy of the models, analytical methods were used for comparison. These methods provided similar results and validated the properties extracted through the FE simulations. The models were implemented to predict the variation in mechanical properties for varying fibre volume fractions, with the results being provided to the mesoscale for analysis.

In addition, the extracted thermal properties were utilised to predict and present the effects of heat transfer across the OGV surface when a thermal element was embedded into the microstructure. This was achieved using the ANSYS Transient Thermal Workbench. The thermal properties, heat flux, and surface temperature showed no significant differences across varying fibre volume fractions, as presented in Table 4.3. However, the time required to reach steady state was influenced by the fibre volume fraction.

Bibliography

[1] B. o. E. Committee on Aeronautics, D. o. E. Environmental Systems, and N. R. C. Physical Sciences, *Commercial Aircraft Propulsion and Energy Systems Research: Reducing Global Carbon Emissions*. The National Academies Press, 09 2016.

[2] Makino Milling Machine Co. Ltd , "Aluminium Outlet Guide Vanes." n.d. [Online]. Available: `https://www.makino.eu/en-us/digital-showroom/aluminium-outlet-guide-vane`. (accessed on: 2021-01-23).

[3] C. Oddy, "Research Engineer Private GKN communication." Private communication, February 2024.

[4] GKN Aerospace, "Innovation." 2024. [Online]. Available: `https://www.gknaerospace.com/en/our-technology/`. (accessed on: 2024-01-16).

[5] Fureho AB, Stena Center Sweden, "Fureho Website." n.d. [Online]. Available: `https://www.fureho.com/`. (accessed on: 2024-01-24).

[6] L. Tong, A. P. Mouritz, and M. Bannister, *3D fibre reinforced polymer composites*. Elsevier, 2002.

[7] C. Oddy, *Macroscale Modelling of 3D-Woven Composites: Inelasticity. Progressive Damage and Final Failure*. PhD thesis, Chalmers University of Technology, 2022.

[8] Y. Guo, K. Ruan, X. Shi, X. Yang, and J. Gu, "Factors affecting thermal conductivities of the polymers and polymer composites: A review," *Composites Science and Technology*, vol. 193, p. 108134, 2020.

[9] C. T. Sun and R. S. Vaidya, "Prediction of composite properties from a representative volume element," *Composites Science and Technology*, vol. 56, 1996.

[10] Z. Xia, Y. Zhang, and F. Ellyin, "A unified periodical boundary conditions for representative volume elements of composites and applications," *International Journal of Solids and Structures*, vol. 40, pp. 1907–1921, 04 2003.

[11] S. Omairey, P. Dunning, and S. Sriramula, "Development of an abaqus plugin tool for periodic rve homogenisation," *Engineering With Computers*, vol. 35, p. 567–577, 04 2019.

[12] DeepL Write (version may 24), DeepL SE, 2023. [Large Language Model]. `https://www.deepl.com/write`.

[13] ChatGPT (version may 24), OpenAI, 2024. [Large Language Model]. `https://openai.com/gpt`.

[14] P. Khokar, "Research Engineer Private Fureho communication." Private communication, February 2024.

[15] A. Doitrand, C. Fagiano, F.-X. Irisarri, and M. Hirsekorn, "Comparison between voxel and consistent meso-scale models of woven composites," *Composites*

Part A: Applied Science and Manufacturing, vol. 73, pp. 143–154, 2015.

[16] H. J. Kim and C. C. Swan, "Voxel-based meshing and unit-cell analysis of textile composites," *International Journal for Numerical Methods in Engineering*, vol. 56, 2003.

[17] P. Tan, L. Tong, and G. P. Steven, "Modeling approaches for 3d orthogonal woven composites," *Journal of Reinforced Plastics and Composites*, vol. 17, no. 6, pp. 555–563, 1998.

[18] J. Hult, H. Bjarnehed, and C. tekniska högskola. Avdelningen för hållfasthetslära, *Styvhet och styrka: grundkurs i kompositmekanik*. Studentlitteratur, 1992.

[19] V. Terentyeva, I. U. Perera, and N. Narendran, "Analyzing theoretical models for predicting thermal conductivity of composite materials for led heat sink applications," in *IES Annual Conference Proceedings*, 2017.

[20] L. E. Nielsen, "The thermal and electrical conductivity of two-phase systems," *Industrial & Engineering Chemistry Fundamentals*, vol. 13, no. 1, pp. 17–20, 1974.

[21] F. Incropera, D. DeWitt, T. Bergman, and A. Lavine, *Incropera's Principles of Heat and Mass Transfer*. John Wiley & Sons, Incorporated, 2017.

A

Appendix 1

A.1 Workflow

The analysis was divided into three subscale FE models (which were heavily reliant on each other) to propose an improved yarn structure, as mentioned in Section 1. ANSYS and Abaqus simulation software were utilised to obtain all results.

The microscale consisted of simulating on a representative volume element (RVE) to find homogenised material properties for the CFRP. The properties were obtained through ANSYS Material Designer simulations on the created RVE. These properties were then validated using analytical solutions and shared with the mesoscale.

The microscale properties were implemented at the mesoscale in conjunction with TexGen for the mesoscale model creation. In ABAQUS, the EasyPBC plugin was used to solve the model for the homogeneous stiffness matrix of the RVE. Material properties acquired from the microscale were implemented as input for solving. Similarly, the mesoscale results were validated using analytical solutions.

Information from the mesoscale was transferred to the macroscale, where an OGV model was subjected to load cases and tested against failure criteria, which were also analytically validated. Macroscale results were fed back to the mesoscale until a mesoscale RVE was produced that could withstand loading without failure.

The data sharing among all models can be visualised in Figure A.1, illustrating the overall workflow of this thesis.

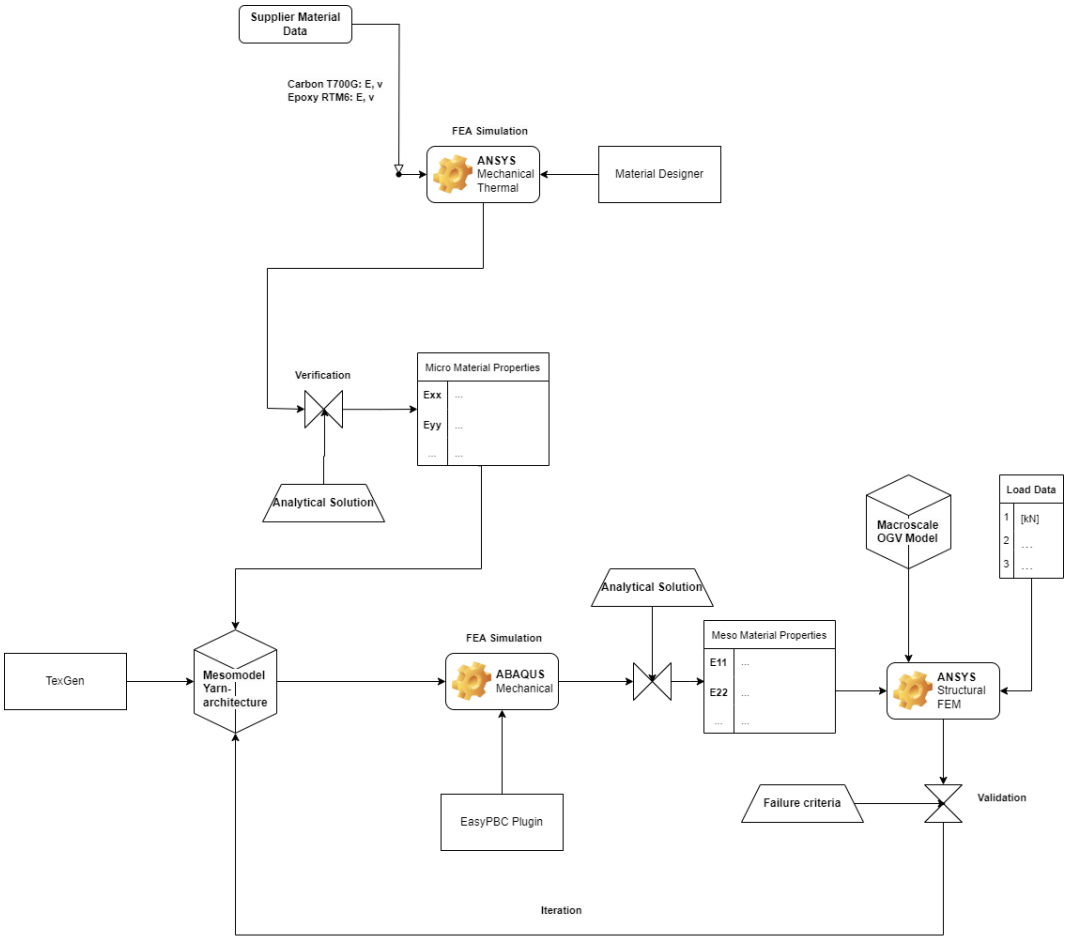

Figure A.1: *Workflow of the thesis.*

A.2 Analytical Modelling of Mechanical Elastic Properties in Composite Materials

A *Mixed Iso-Stress* and *Mixed Iso-Strain* based unit cell modelling scheme can be used to predict elastic mechanical properties for 3D orthogonal non-woven composite materials [17].

By considering a piece of material at the mesoscale from a 3D orthogonal non-woven composite, see Figure A.2a, where the three yarn groups of assumed rectangular cross-sectional area are placed in the orthogonal directions in the coordinate system [*1*, *2*, *3*], the marked volume (in grey) can be treated as a unit cell (shown in Figure A.2b)

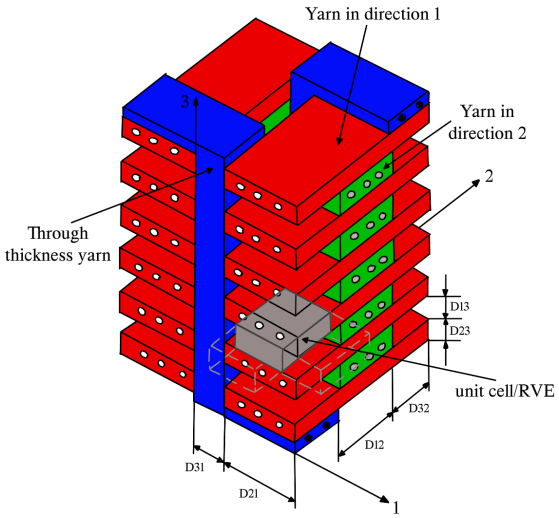

(a) *3D orthogonal non-woven composite.*

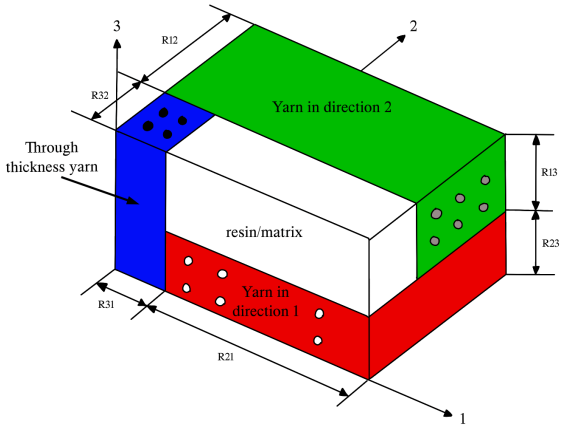

(b) *Unit cell/RVE.*

Figure A.2: *3D orthogonal non-woven composite and RVE, inspiration taken from [6].*

The unit cell can further be subdivided into four cubic blocks as shown in Figure A.3. It is clear that the properties of the unit cell can be evaluated by estimating the properties of each of the four blocks. Figure A.4 illustrates all of the three possible ways of assembling each block consisting of two sub-blocks A and B.

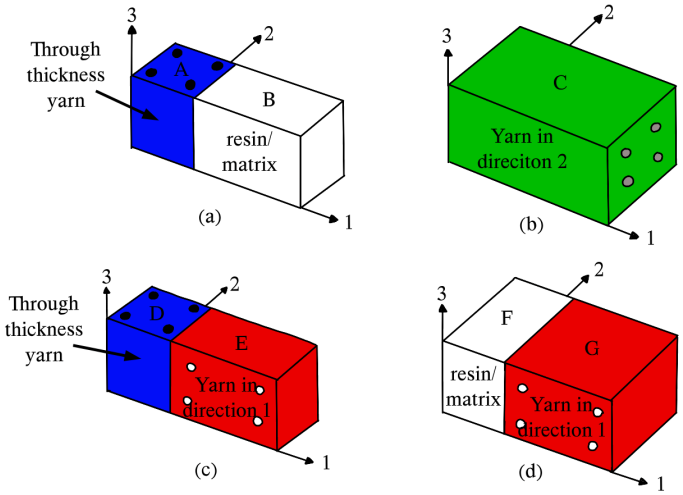

Figure A.3: *Unit cell/RVE split up into four cubic blocks, inspiration taken from [6].*

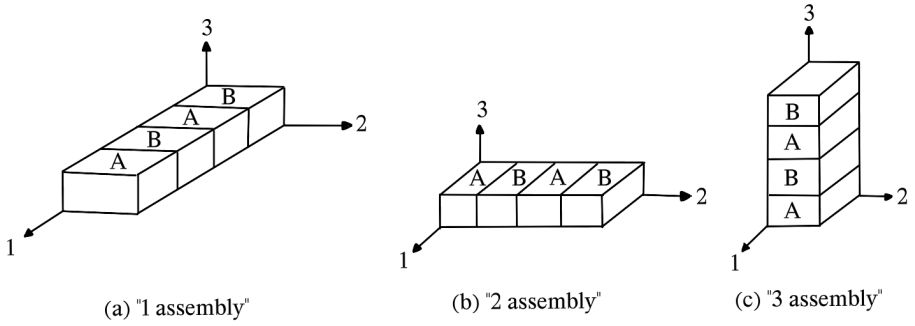

Figure A.4: *The three possible ways of assembling each block consisting of two sub-blocks A and B, inspiration taken from [6].*

The "1-assembly" consists of N^A blocks of material A and N^B blocks of material B in the x-direction. The overall material properties are given via the following equations:

$$\begin{aligned}
C_{11}^S &= \frac{C_{11}^A C_{11}^B}{N^A V^A C_{11}^B + N^B V^B C_{11}^A},\ C_{12}^S = C_{11}^S \left[\frac{N^A C_{12}^A V^A}{C_{11}^A} + \frac{N^B C_{12}^B V^B}{C_{11}^B}\right] \\
C_{13}^S &= C_{11}^S \left[\frac{N^A C_{13}^A V^A}{C_{11}^A} + \frac{N^B C_{13}^B V^B}{C_{11}^B}\right],\ C_{22}^S = N^A C_{22}^A V^A + N^B C_{22}^B V^B \\
C_{23}^S &= N^A C_{23}^A V^A + N^B C_{23}^B V^B,\ C_{33}^S = N^A C_{33}^A V^A + N^B C_{33}^B V^B \\
C_{44}^S &= N^A C_{44}^A V^A + N^B C_{44}^B V^B,\ C_{55}^S = \frac{C_{55}^A C_{55}^B}{N^A V^A C_{55}^B + N^B V^B C_{55}^A} \\
C_{66}^S &= \frac{C_{66}^A C_{66}^B}{N^A V^A C_{66}^B + N^B V^B C_{66}^A}
\end{aligned} \tag{A.1}$$

where N^A and N^B are the numbers of sub-blocks A and B within a strip, V^A and V^B are the volume fractions of sub-block A and sub-block B in a strip respectively and C_{ij}^A, C_{ij}^B, C_{ij}^S are the stiffness constants for a sub-block A, a sub-block B and a strip respectively.

The overall material properties for the "2-assembly" block are given by the following equations:

$$\begin{aligned}
C_{11}^S &= N^A C_{11}^A V^A + N^B C_{11}^B V^B,\ C_{12}^S = C_{22}^S \left[\frac{N^A C_{12}^A V^A}{C_{22}^A} + \frac{N^B C_{12}^B V^B}{C_{22}^B}\right] \\
C_{13}^S &= N^A C_{13}^A V^A + N^B C_{13}^B V^B,\ C_{22}^S = \frac{C_{22}^A C_{22}^B}{N^A V^A C_{22}^B + N^B V^B C_{22}^A} \\
C_{23}^S &= C_{22}^S \left[\frac{N^A C_{23}^A V^A}{C_{22}^A} + \frac{N^B C_{23}^B V^B}{C_{22}^B}\right],\ C_{33}^S = N^A C_{33}^A V^A + N^B C_{33}^B V^B \\
C_{44}^S &= \frac{C_{44}^A C_{44}^B}{N^A V^A C_{44}^B + N^B V^B C_{44}^A},\ C_{55}^S = N^A C_{55}^A V^A + N^B C_{55}^B V^B \\
C_{66}^S &= \frac{C_{66}^A C_{66}^B}{N^A V^A C_{66}^B + N^B V^B C_{66}^A}
\end{aligned} \tag{A.2}$$

Lastly the overall material properties for the "3-assembly" block are given by the following equations:

$$
\begin{aligned}
C_{11}^S &= N^A C_{11}^A V^A + N^B C_{11}^B V^B,\ C_{12}^S = N^A C_{12}^A V^A + N^B C_{12}^B V^B \\
C_{13}^S &= C_{33}^S \left[\frac{N^A C_{13}^A V^A}{C_{33}^A} + \frac{N^B C_{13}^B V^B}{C_{33}^B} \right],\ C_{22}^S = N^A C_{22}^A V^A + N^B C_{22}^B V^B \\
C_{23}^S &= C_{33}^S \left[\frac{N^A C_{23}^A V^A}{C_{33}^A} + \frac{N^B C_{23}^B V^B}{C_{33}^B} \right],\ C_{33}^S = \frac{C_{33}^A C_{33}^B}{N^A V^A C_{33}^B + N^B V^B C_{33}^A} \\
C_{44}^S &= \frac{C_{44}^A C_{44}^B}{N^A V^A C_{44}^B + N^B V^B C_{44}^A},\ C_{55}^S = \frac{C_{55}^A C_{55}^B}{N^A V^A C_{55}^B + N^B V^B C_{55}^A} \\
&\qquad C_{66}^S = N^A C_{66}^A V^A + N^B C_{66}^B V^B
\end{aligned}
\tag{A.3}
$$

The elastic constants for the blocks in Figure A.3 a, c and d can be evaluated using the 1-assembly equations together with the stiffness constants for the yarns and the matrix. The stiffness constant for the combined block a and b as well as c and d can in turn be evaluated using the 2-assembly equations. The overall properties for the unit cell can then be obtained using the 3-assembly equations.

DEPARTMENT OF INDUSTRIAL AND MATERIALS SCIENCE
CHALMERS UNIVERSITY OF TECHNOLOGY
Gothenburg, Sweden
www.chalmers.se

CHALMERS
UNIVERSITY OF TECHNOLOGY